Polarimetry and Interferometry Applications

Wolfgang Keydel

Microwaves and Radar Institut
DLR Oberpfaffenhofen
Contact Address:
Mittelfeld 4,D-82229 Hechendorf Germany

Tel.:49-8152-980 523
E-mails: wolfgang@keydel.com
wolfgang.keydel@dlr.de

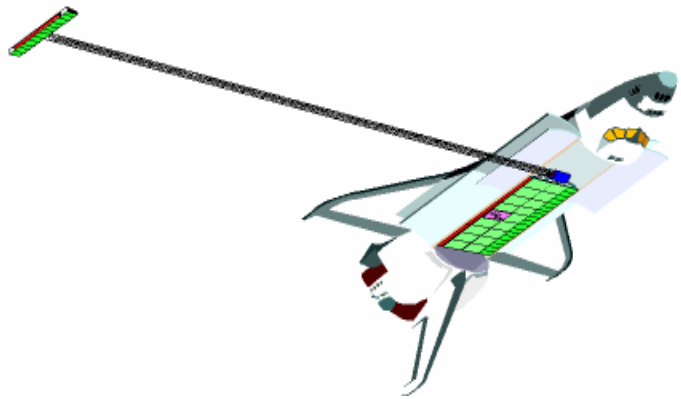

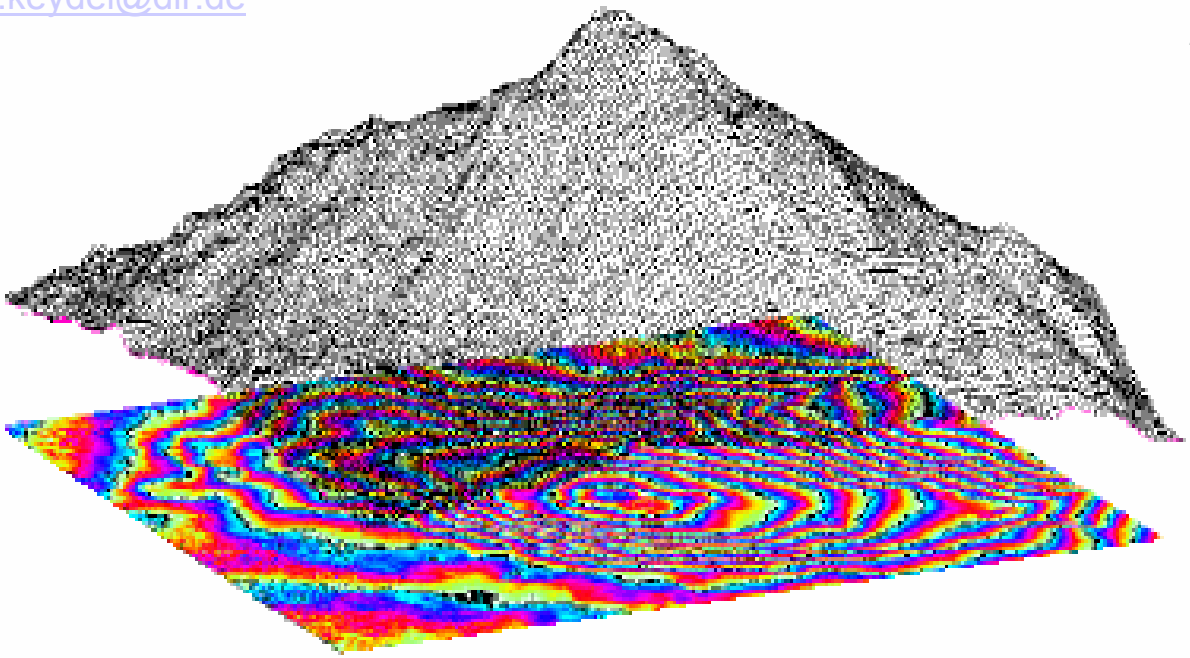

Goal

Point out exemplary some Application Possibilities of the Interferometric & to some extent Polarimetric Techniques & Systems considered & presented in the forgoing respective Lectures in order to deepen & fasten the Auditories Understanding & Comprehension

★

Offer a Glance into a Selection of Representative Activities in the Domains of

Scientific , Commercial, & Operational Applications

of

Interferometry & Polarimetry

Safety for Air Traffic

Disaster management

Telecommunications

Applications for Digital Height Models

Infrastructure planning

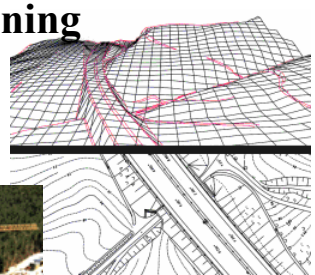

Hydrology

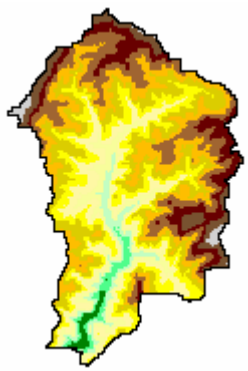

Quellenangabe

Application Areas and Specific User Requirements

Driver for research & development of all SAR Technique, Technology & Systems

Parameter	Cartography	Disaster Management	Urban Mapping	Military
Frequency	L, C, X	L,C,	L, C, X	L, X
Polarization		Quad	Quad	Quad
Incidence Interval	Variable	Variable 20° - 60°	Variable 20° - 60°	Variable 20° - 60°
Spatial Resolution	3 m – 5 m	0.5 m – 100m	1m – 5 m	0,1 m -10 m
Swath Width	Variable	Variable 10km -350 km	40 km–100 km	5km – 100km
Revisit Time	1 Year…. Application	1 hr – 1 day	Yearly	1 hr –1 day
Data access	Regularly	Real Time	Regularly	Real Time

Quellenangabe

Parameter	Agriculture	Forestry	Geology	Hydrology	Oceanography
Frequency	L,C	L, C, X	L, C, X	L, C, X	L,C
Polarization	quad	quad	dual/quad	Dual/quad	Quad
Incidence Interval	25° – 45°	20° - 45°	20° -60°	20°- 45°	20° -45°
Spatial Resolution	3m-30m	10 m	3m – 10m	3m – 10m	30 m-1 km
Swath Width	30 km	Variable	Variable 40 km – 100 km	Variable 100 km	Variable 25 km-350 km
Revisit Time	≤ 15 days	0.3 - 1 Year	Seasonal	10 days – 15 days	1 day
Data access	Real Time	Regularly	Regularly	Regularly	Real Time
Additional		Tomography			Raw Data

Quellenangabe

SAR Interferometry Applications & User

- Creation of Land Deformation Maps with Millimetre Accuracy
- Generation of Digital Elevation Models with Meter Accuracy,
- Improved Target Recognition by Creation of 3D Images of Targets
- Improved Land Use Classification by exploiting Coherence Measurements,

  Measurement of Current Fields & Moving Target Indication
- Economical & Operational Importance for Constructors
  (Building a Tunnel can cause Unwanted Deformation),
- Governments (Dike Monitoring, Disaster Monitoring),
- Military (Target Detection,Identification, Classificationm, Area Exploration
- Governments & Companies creating Georectified SAR Imagery
  (Need for Topographic Maps), etc.

Quellenangabe

SAR Polarimetry Applications

Polarimetry offers Maximal Information an Electromagnetic Wave can carry.

Most Modern Civil & Military Applications require full Polarimetric Systems.

Polarization will Improve exemplary:

Ice Detection &Classification,

Man Made Target Detection & Classification,

Crop Monitoring & Clasification etc..

⋮

Commercial Aspects are widely in the Foreground

Quellenangabe

Polarimetry

Polarization is the Orientation of the Electric Vector *(E)* in an Electro Magnetic Wave, frequently "Horizontal" (H) or "Vertical" (V) in conventional imaging radar systems. Polarization is Established by the Antenna.

Complete State of scattered Electromagnetic Wave described by the Scattering Matrix S, which connects the Received Field Vector E_r with the Transmitted Field Vector E_t. (Börner)

$$\begin{bmatrix} E_H^r \\ E_V^r \end{bmatrix} = [S] \begin{bmatrix} E_H^t \\ E_V^t \end{bmatrix} = \begin{bmatrix} S_{HH} & S_{HV} \\ S_{VH} & S_{VV} \end{bmatrix} \begin{bmatrix} E_H^t \\ E_V^t \end{bmatrix}$$

Scattering Matrix Decomposition into 3 Components (Example Sperical Basis):

$$[S] = e^{j\varphi} \left\{ e^{j\varphi_s} k_s [S_{sphere}] + k_d [S_{diplane}] + k_k [S_{helix}] \right\}$$

Quellenangabe

Scattering Matrix

$$\vec{E} = \vec{E}_0 \frac{e^{-\alpha r}}{kr} e^{-j(\omega t + \varphi)} \qquad \ldots \alpha = jk + \gamma$$

$$E_H^{scat} = S_{HH} E_H^{inc} + S_{HV} E_V^{inc}$$

$$E_V^{scat} = S_{VH} E_H^{inc} + S_{VV} E_V^{inc}$$

$$\vec{E}_{scat} = \begin{pmatrix} E_H^{scat} \\ E_V^{scat} \end{pmatrix} = \begin{pmatrix} S_{HH} & S_{HV} \\ S_{VH} & S_{VV} \end{pmatrix} \begin{pmatrix} E_H^{inc} \\ E_V^{inc} \end{pmatrix} = (S)\, \vec{E}_{inc}$$

$$S_{i,k} = \sqrt{\sigma_0^{i,k}}\, e^{j\varphi_{i,k}}$$

Quellenangabe

Basis Matrices

A generic Matrix is decomposable into Basis Matrices

$$[S] = \begin{bmatrix} S_{HH} & S_{HV} \\ S_{VH} & S_{VV} \end{bmatrix}$$

$$\begin{bmatrix} a+b & c \\ c & a-b \end{bmatrix} = a\begin{bmatrix} 1 & 0 \\ 0 & 1 \end{bmatrix} + b\begin{bmatrix} 1 & 0 \\ 0 & -1 \end{bmatrix} + c\begin{bmatrix} 0 & 1 \\ 1 & 0 \end{bmatrix}$$

$$a + b = S_{HH} \; ; a - b = S_{VV}$$

$$a = S_{HH} + S_{VV} \; ; b = S_{HH} - S_{VV} \; ; c = S_{HV} = S_{VH}$$

$$\textit{Scattering Vector } \vec{k} = (a,b,c) = (S_{HH} + S_{VV} ; S_{HH} - S_{VV} ; S_{HV})$$

Quellenangabe

Pauli Distribution

Single Bounce, odd

Double Bounce, even

Volume Scattering, diffuse

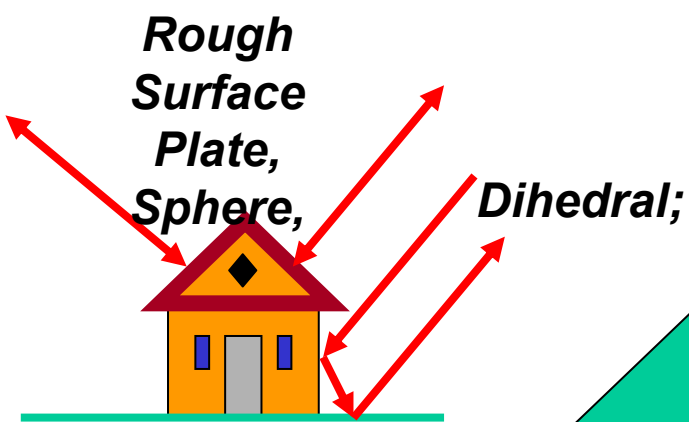

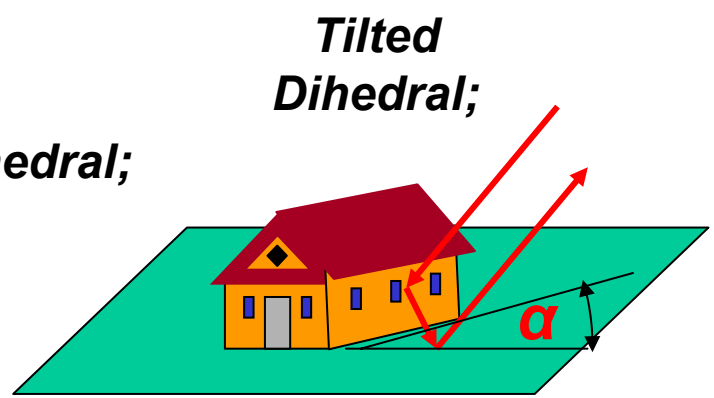

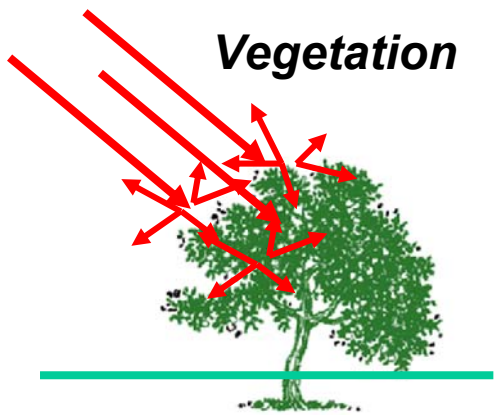

$$S_{odd} = \begin{bmatrix} 1 & 0 \\ 0 & 1 \end{bmatrix}, \quad S_{even} = \begin{bmatrix} \cos 2\alpha & \sin 2\alpha \\ \sin 2\alpha & \cos 2\alpha \end{bmatrix} \rightarrow \quad S_{diff} = \begin{bmatrix} 0 & 1 \\ 1 & 0 \end{bmatrix}$$

Scattering Vector $\vec{k}_{scat} = (k_{odd}, k_{even}, k_{diff}) = (S_{HH} + S_{HV}, S_{HH} - S_{HV}; 2S_{HV})$

Quellenangabe

Polarimetric Image of the E-SAR System in L-Band

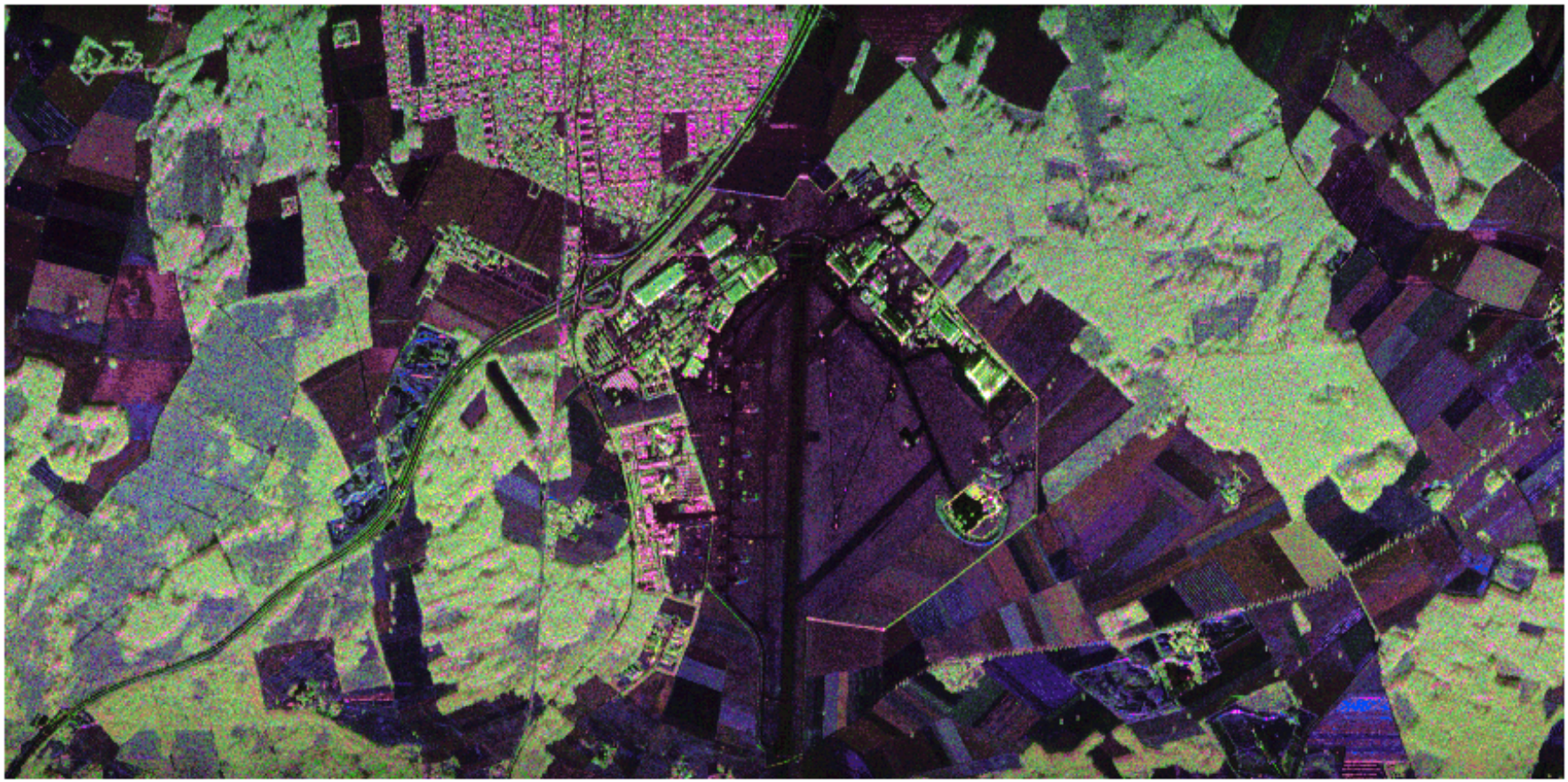

HH +VV (single bounce)

HH - VV (double bounce)

HV+VH (volume scattering)

$$S_1 = \begin{bmatrix} 1 & 0 \\ 0 & 1 \end{bmatrix}, S_2 = \begin{bmatrix} \cos 2\alpha & \sin 2\alpha \\ \sin 2\alpha & \cos 2\alpha \end{bmatrix}, S_{dfiffus} = \begin{bmatrix} 0 & 1 \\ 1 & 0 \end{bmatrix}$$

Example for three-dimensional *'POL-IN-DEM'* information

E-SAR, L - Band

VV-Polarization

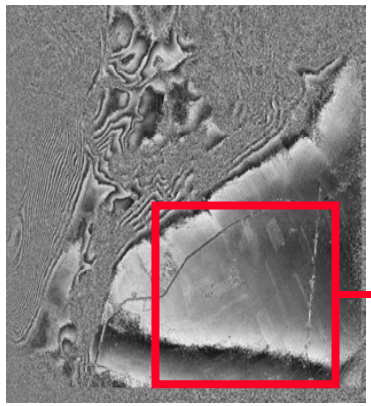

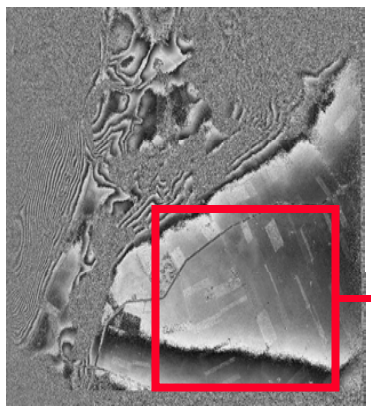

HH-Polarization

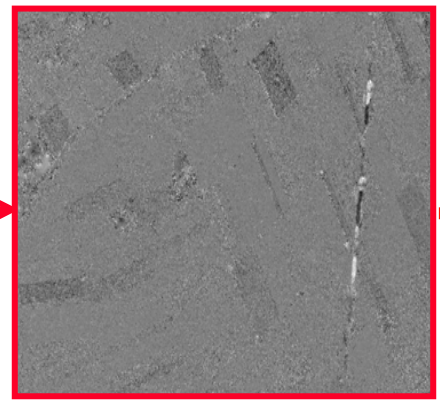

Δ- Polarization (HH-VV)

Vegetation with vertical Structures

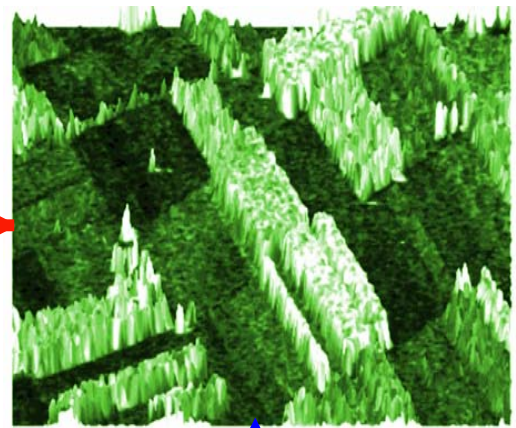

Scattering Matrix → Coherent Decomposition in orthogonal Parts

Combination of Polarimetry and Interferometry

SAR Polarimetry (PolSAR)

Allows the decomposition of different scattering processes occurring inside the resolution cell

SAR Interferometry (InSAR)

Allows the location of the effective scattering center inside the resolution cell

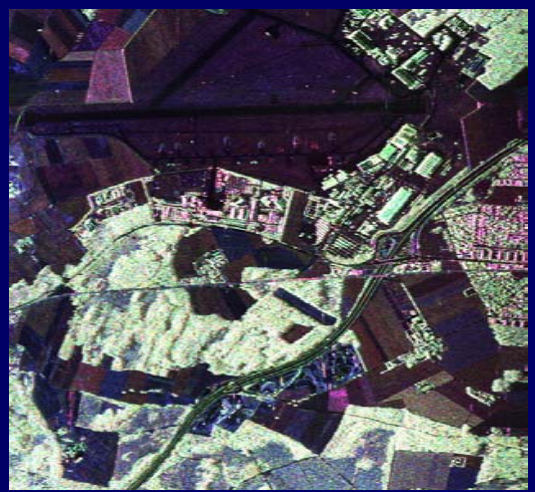

Pol. Pauli Decomposition RGB

SAR Image

InSAR DEM

Polarimetric SAR Interferometry (Pol-InSAR)

Potential to separate in height different scattering processes occurring inside the resolution cell.

<u>Sensitivity to the vertical distribution of the scattering mechanisms</u>

Allows the investigation of 3D structure of volume scatterers

The Combination of Polarimetry and Interferometry

SAR Polarimetry ← Phase sensitivity → SAR Interferometry

Sensitive to scatterers shape, orientation and dielectric properties Allows decomposition of different scattering processes occurring inside the resolution cell

Established technique for terrain topography estimation allows Location of scattering centers inside the resolution cell

Polarimetric SAR Interferometry

Potential to separate in height different scattering processes occuring inside the resolution cell.

↓

Sensitivity to the vertical distribution of the scattering mechanisms

Allows the investigation of 3D structure of volume scatterers recovering co-registered textural plus spatial properties simultaneously

Central Part: Coherence

Quellenangabe

Applications for Digital Elevation Models DEM)

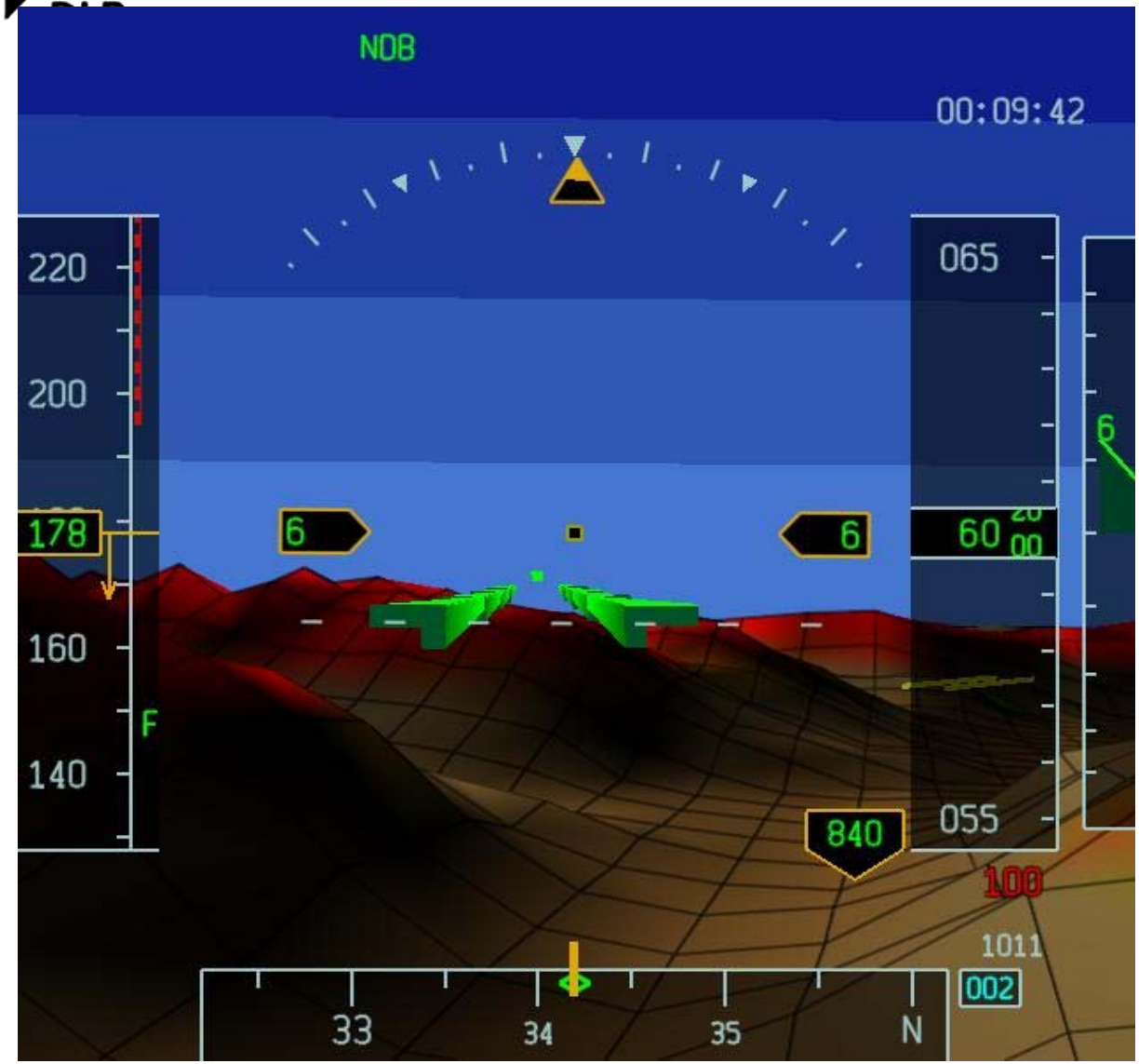

Example: Air traffic Safety

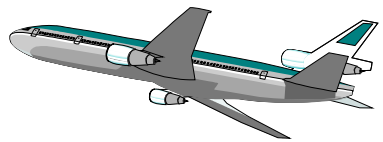

"Virtual Cockpit"

- **Precise Information about Aircraft Position by GPS**
- **Precise Information about Topography below from global, consistent DEM (SRTM)**

Quellenangabe

Hydrology: Water Flow Simulation

Globe-30 DEM

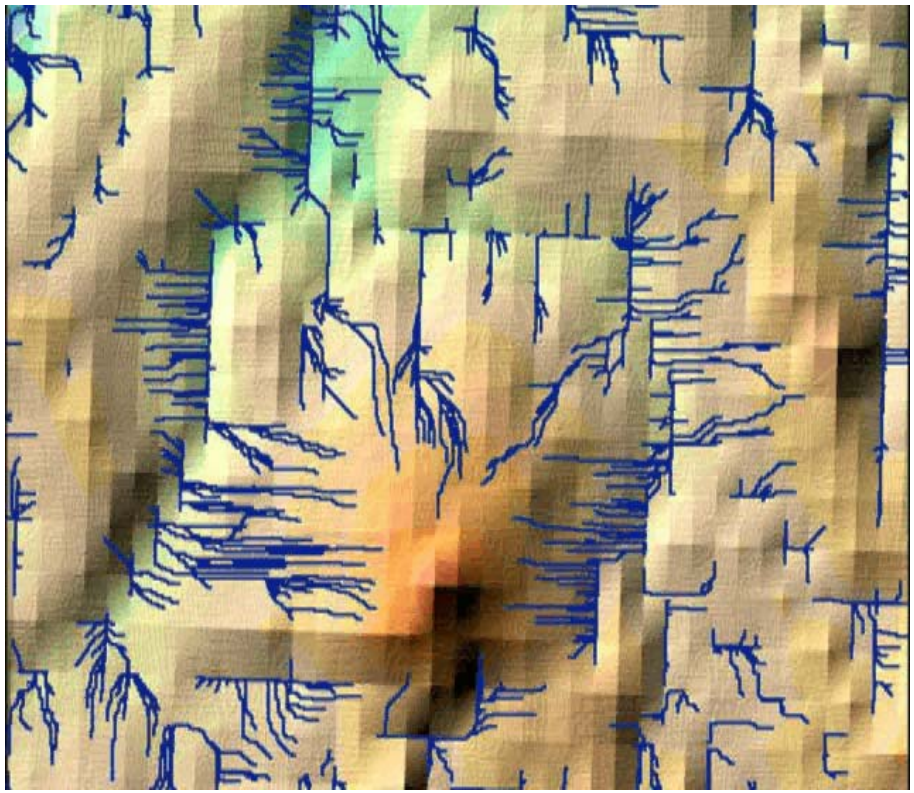

SRTM DEM

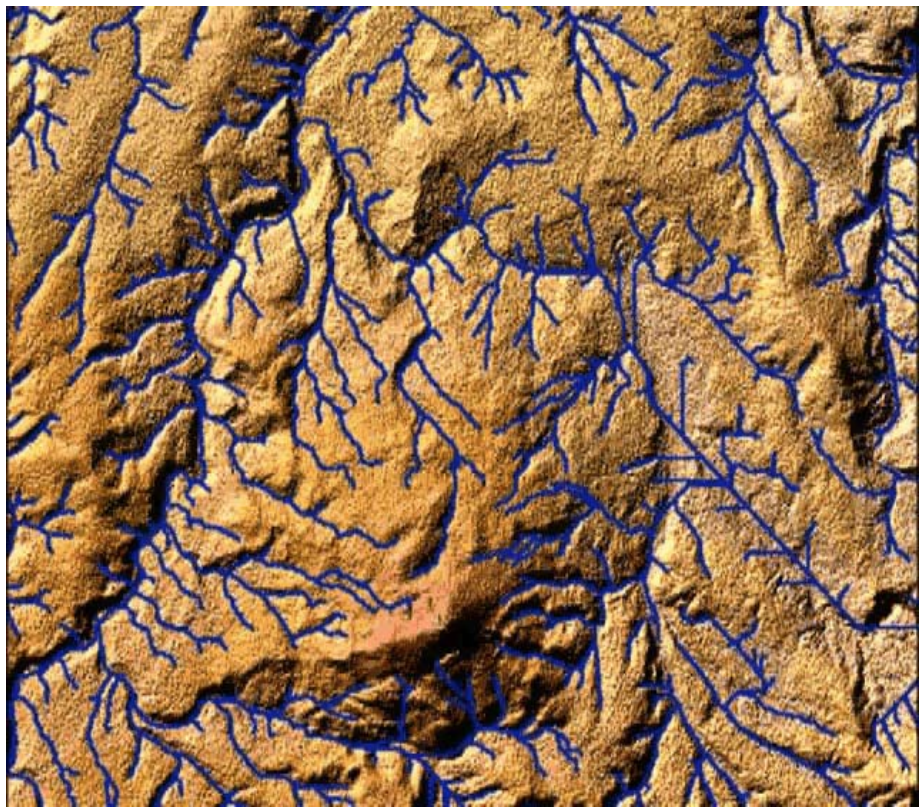

Quellenangabe

Example: Polarimetric Ice, Water, & Land Classification

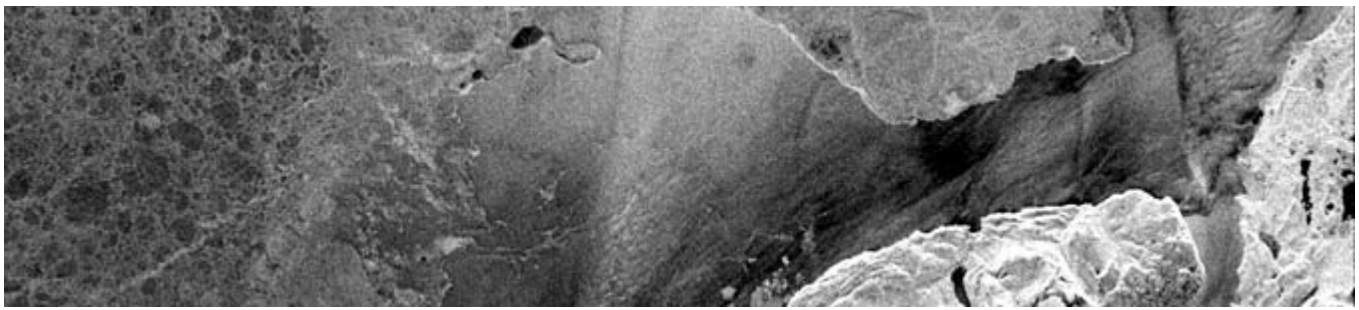

HH Ice Type

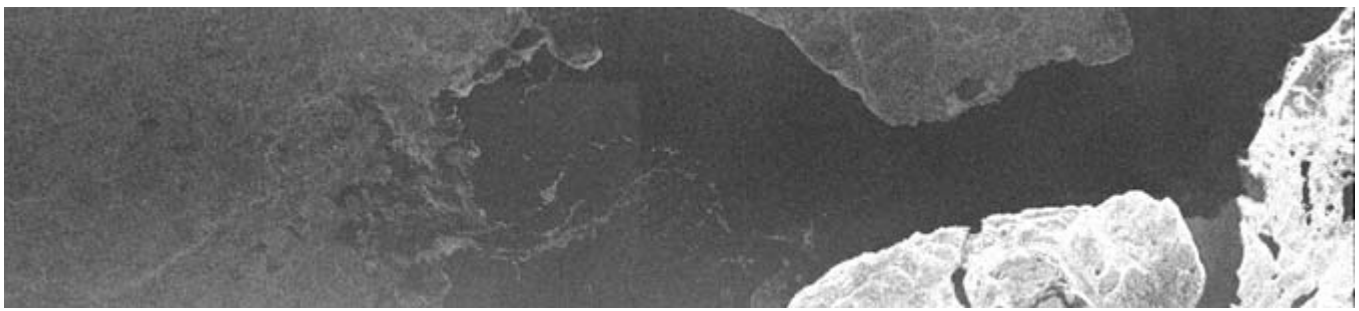

HV Ice Edge

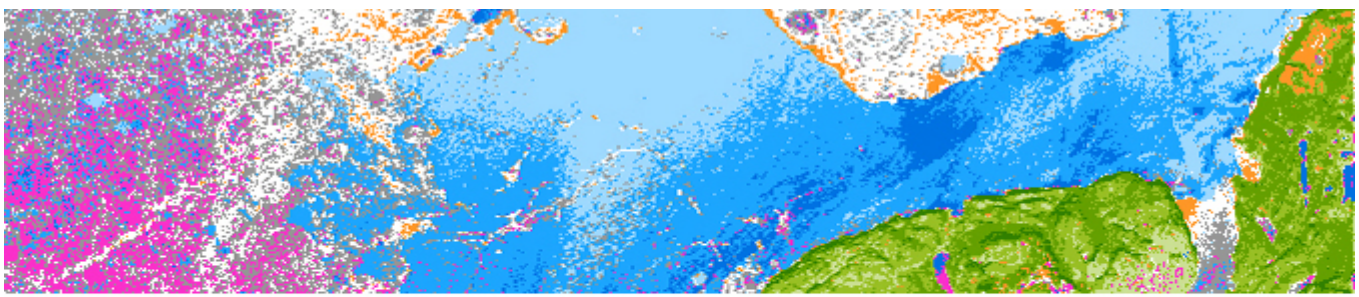

H/A/α Maximum Likelihood Classification Results After Five Iterations

Colour code (5 null classes)

land 1
land 2
land 3
land 4

water 1
water 2
water 3

sea ice 1
sea ice 2
sea ice 3
sea ice 4

Courtesy Mc Donald Dettwiler & Associates

www.rsi.ca/rsic/ice/eoadp.asp

Military Use of Interferometry and Polarimetry

"The war is father of everything"

Task of Military Reconnaissance Systems

"Assist the Military Leaders in the Early Detection of Crisis Prevention & Crisis Management Efforts, Support the Top Military Leadership to plan and prepare military operations and Support Deployed Forces in the Timely Collection of Current Intelligence Information".
(Col. F. Kriegel on "European Satellites for Security" in Brussels, June 2002),

One of the Biggest Tasks For Tactical & Strategic Consideration to get Things Timely, Safely & Efficiently at the Battlefield.

Interferometry & Polarimetry driven intensively by Military Requirements. For Target Detection, Recognition, Identification & Classification full polarimetric information is indispensable.

Decomposition Theorems excellently suited for Target Exploration under Vegetation Layers due to Foliage Penetration Capability of dm-Waves etc.

Quellenangabe

Polarimetric & Interferometric SAR indispensable

for Collecting Terrain Information like Engineering Resources, Trafficability, Obstacles, Visibility, Camouflage, Concealment Potential, Information on Camping Ground, Water Supply etc.

Systems mounted on Aircrafts, UAV's, & Satellites allow actual updating of already existing Maps or establishing of new Feature Maps in Real Time.

Example: DEM's

Military Topographic Maps are most important for Terrain Evaluation.

Aircraft & Helicopter Missions in mountainous ore even hilly Terrain can be supported in Advance & during the Mission with DEM of respective Areas.

Soil Moisture Maps help to identify the best Way for off Road Movements etc. (necessary also for establishing Communication Links etc).

US NIMA has financed the SRTM Mission

illuminating the Importance of DEM's for Military Purposes.

Quellenangabe

Flight over unknown Area

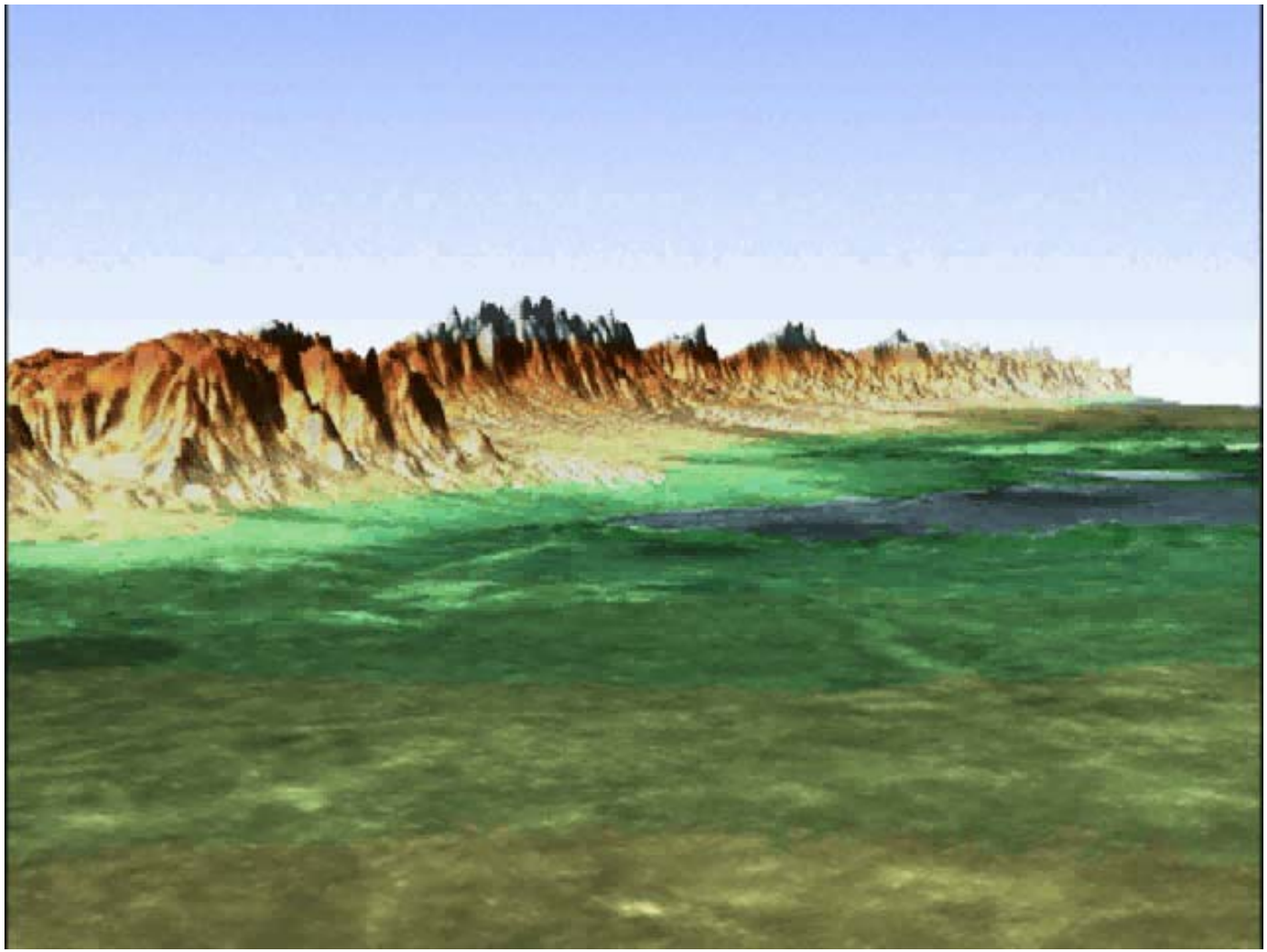

Quellenangabe

Technical Applications
SRTM Systems Operation Geometry

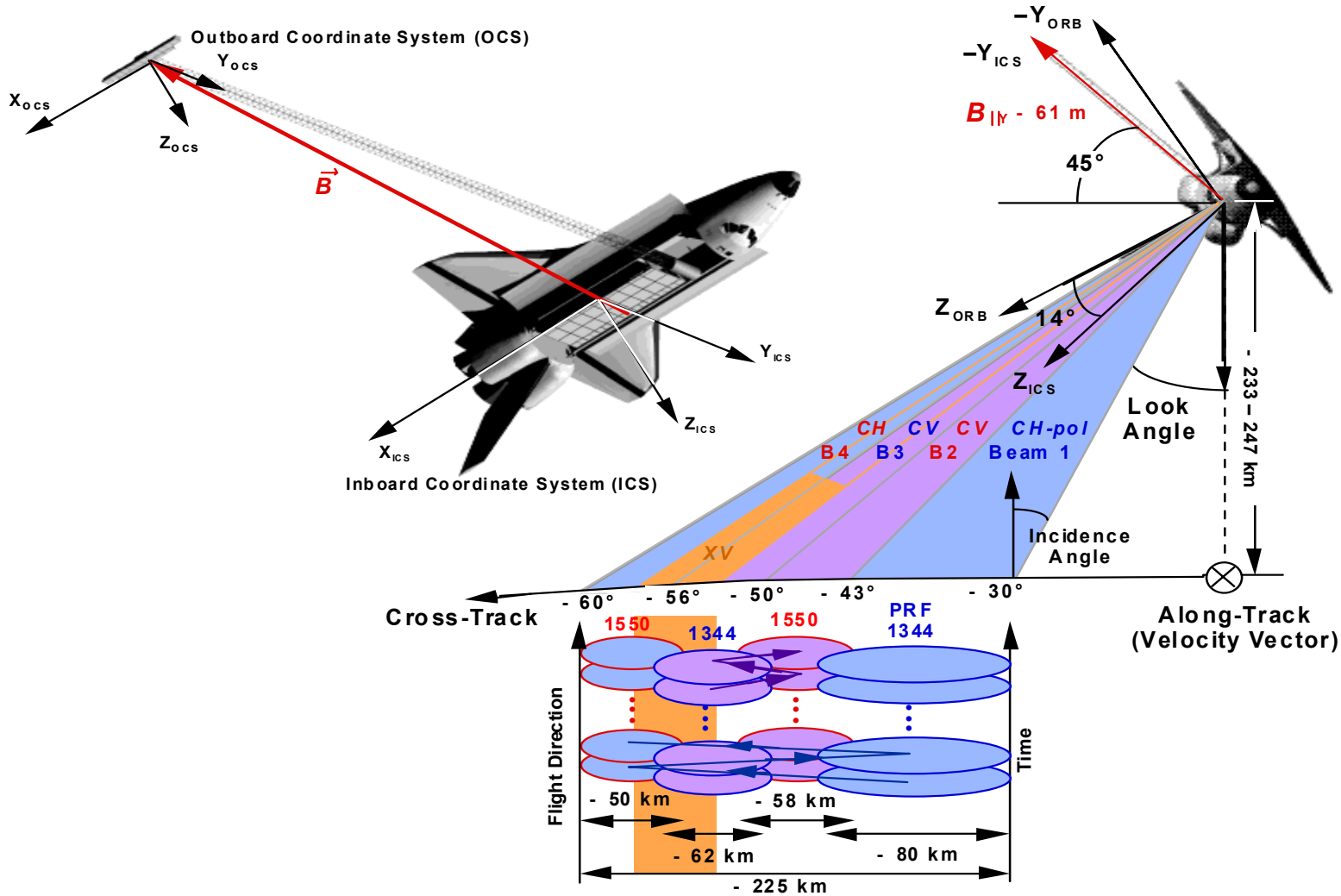

Courtesy JPL

Quellenangabe

Technical Applications
SRTM Systems Operation Geometry

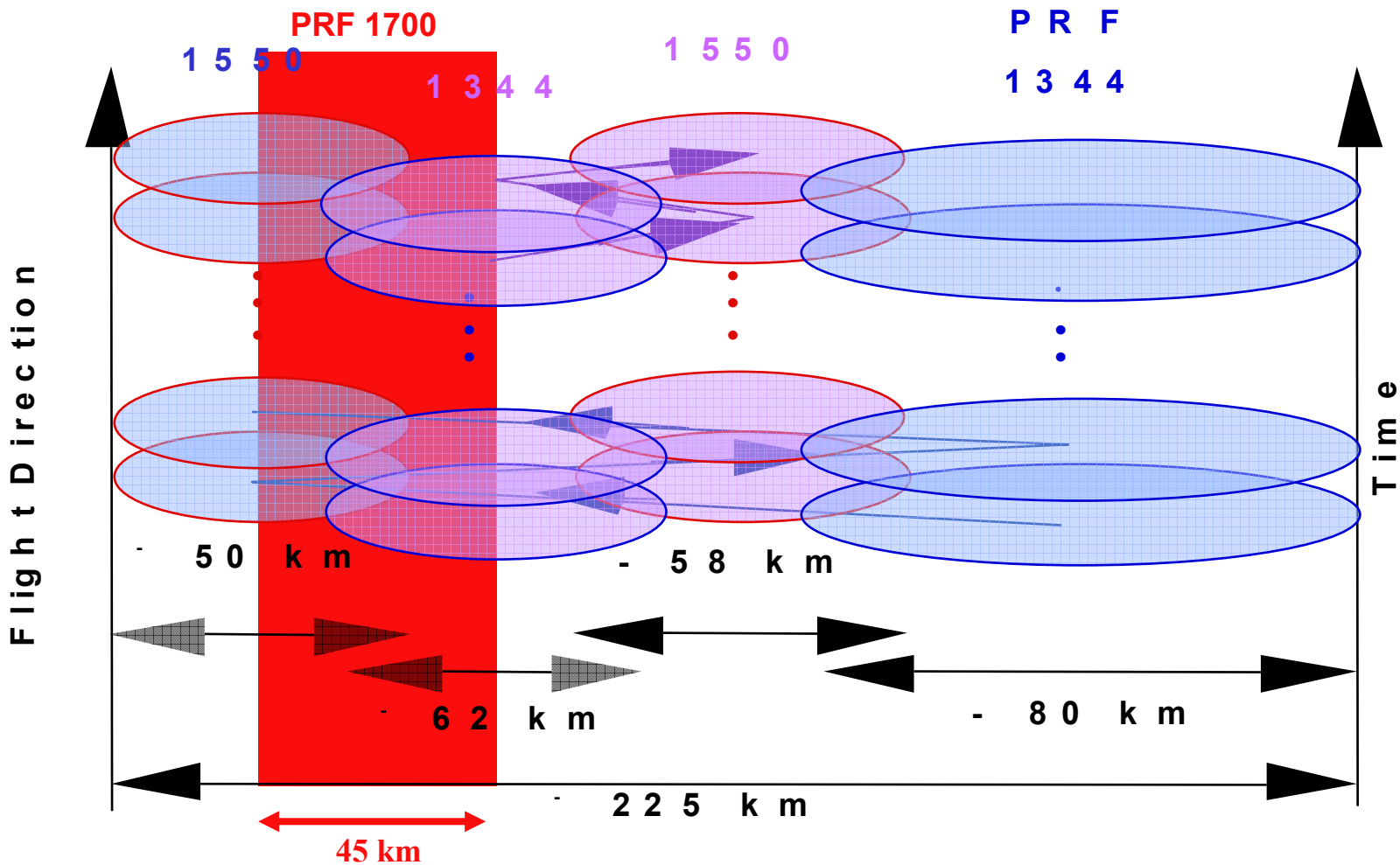

Quellenangabe

Tomography

Principle of Tomography

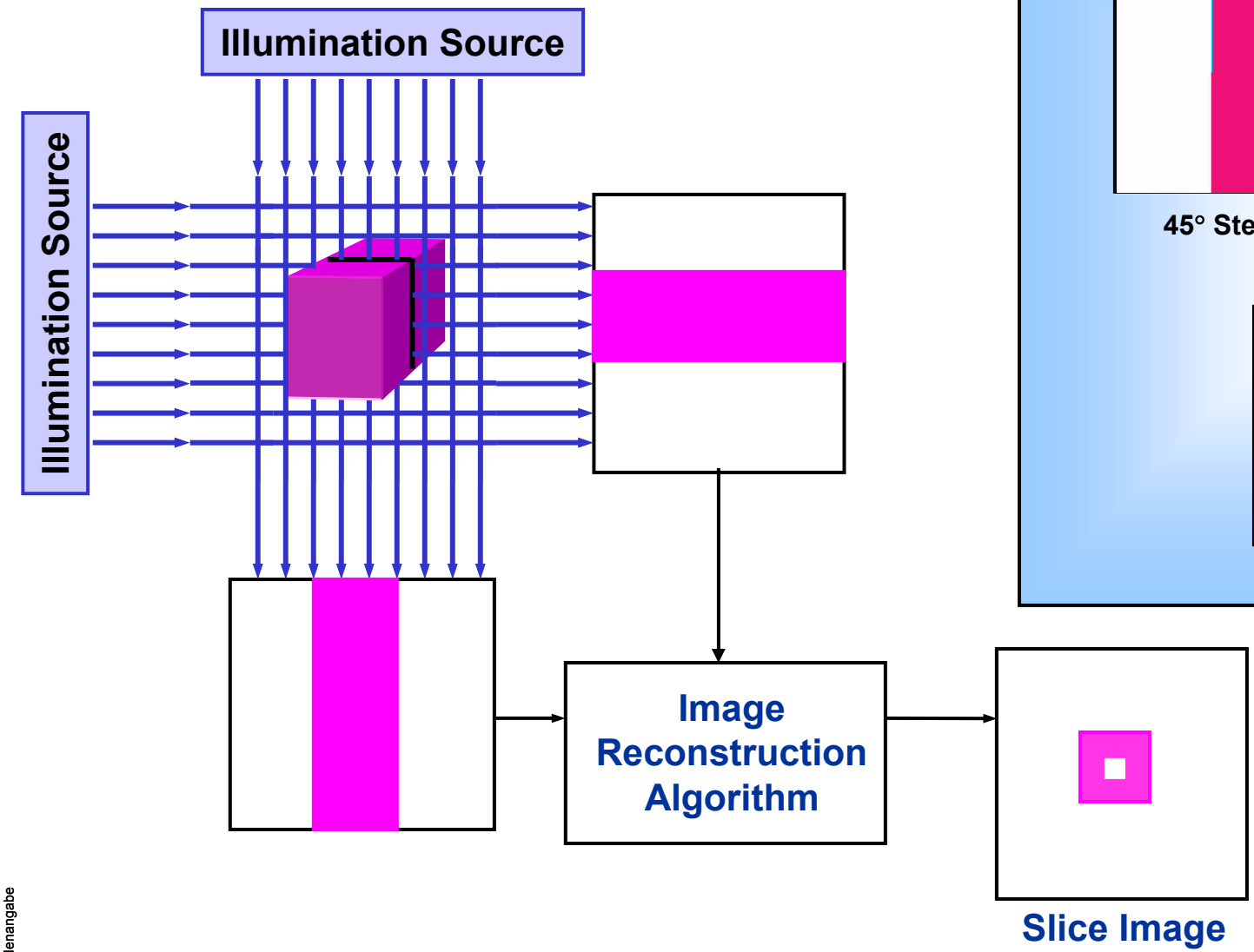

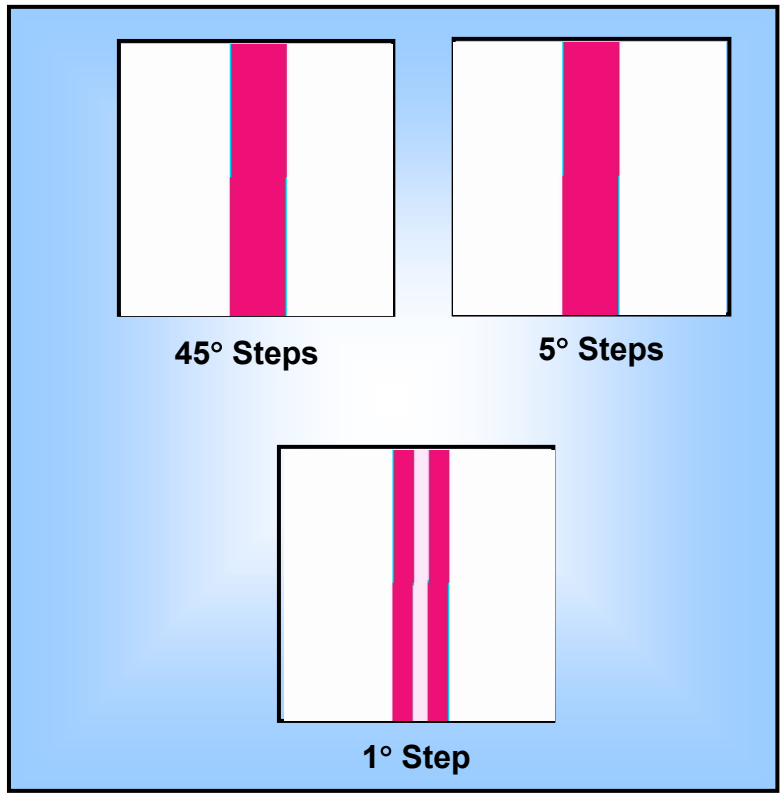

Polarimetric E-SAR Image, L-Band

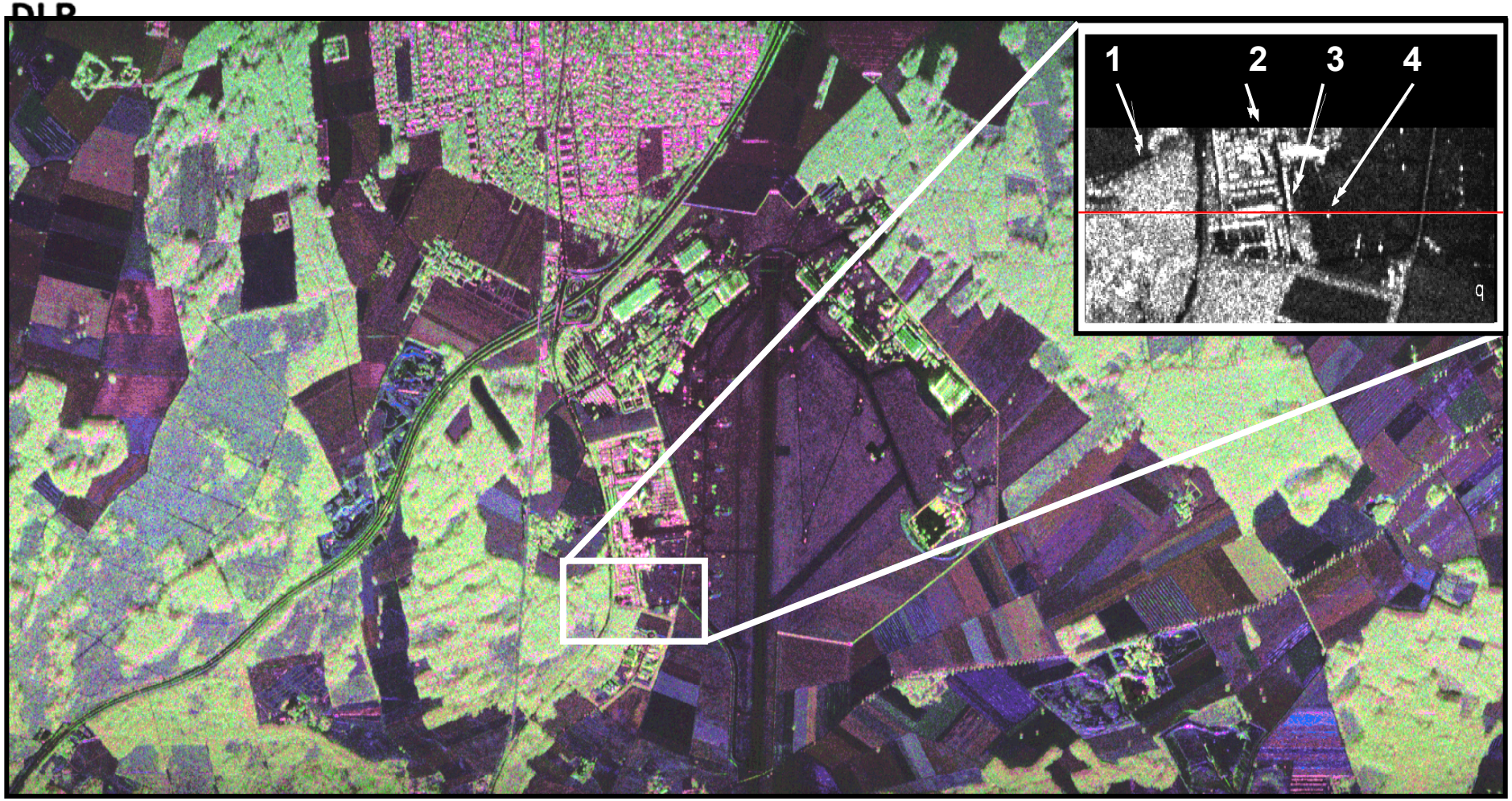

HH +VV (single bounce)

HH - VV (double bounce)

HV+VH (volume scattering)

1) spruce forest
2) buildings
3) cars
4) corner reflector

Quellenangabe

SAR-Tomography

2-dimensional image of a cut (τομή) through a 3-dimensional Objekt

Multiple parallel repeat-pass POL-IN-SAR imaging

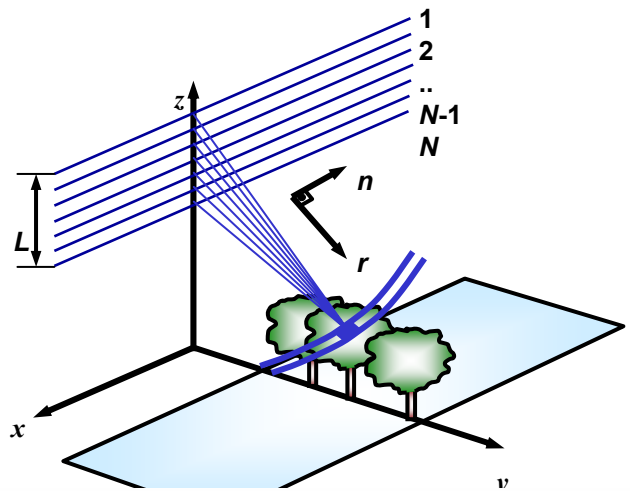

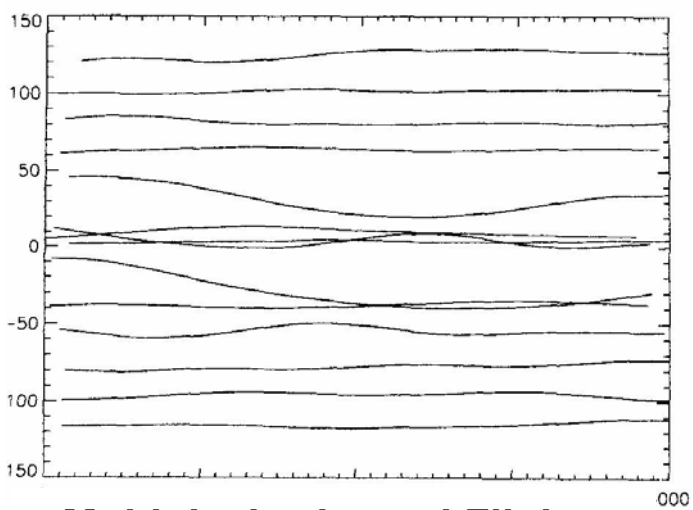

Multiple horizontal Flights

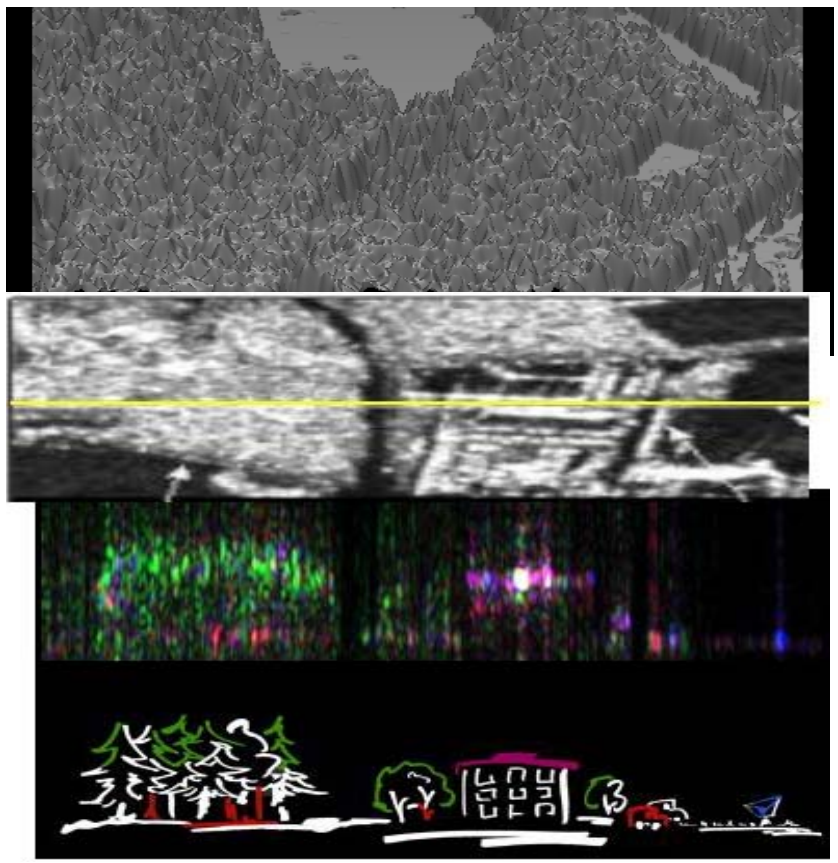

Tomography for Scattering Analysis

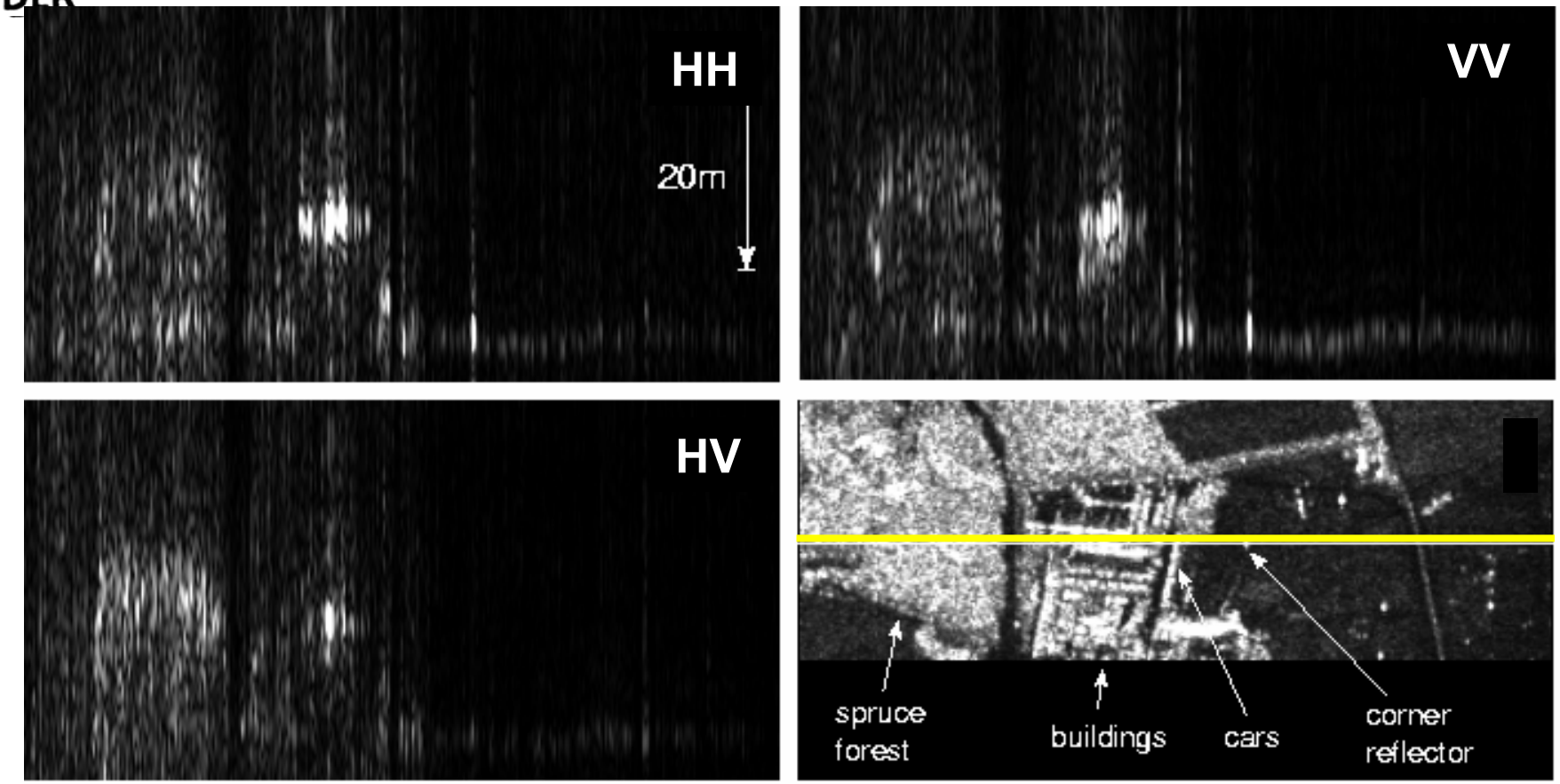

Scattering Mechanisms along Yellow Line at different Altitudes & Polarizations. Buildings Roof is Bright: Bright HH and VV Single Bounce is the Corner Reflector. Double Bounces at Parts of the Buildigs Roof & the Lower Parts of Trunks, Volume Scattering dominates in Tree Crowns & Under Story

[Reigber, Moreira, First Demonstration of Airborne SAR Tomography IEEE Trans. GRSS, vol 38. No. 5, Sept: 2000]

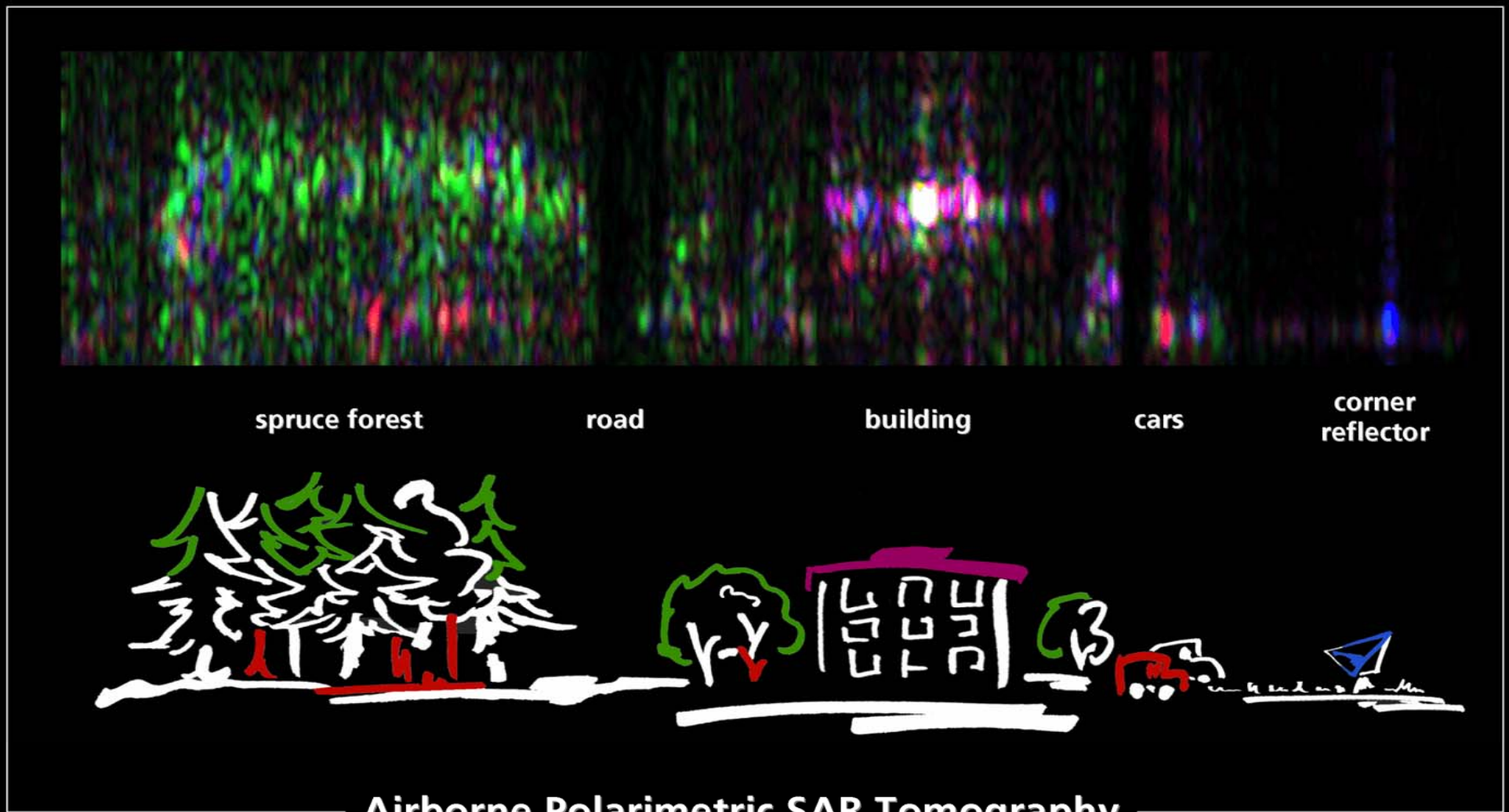

Airborne Polarimetric SAR Tomography

Upper image: Polarimetric color composite (L-band) of a tomographic slice in the height/azimuth-direction
HH+VV, HH-VV, 2*HV

Lower image: Schematic view of the imaged area

Use of Interferometry for Building Measurements

Using Terrain Elevation Data from Interferometry in Combination wth Gray Value Images & Object Shadows Allows Building Mapping

Accuracy of Buildings Mapped from Sensor with 30 cm Pixels about ± 3 Pixels or ± 1 m.

2 Overlapping Data Sets are Definitely Needed.

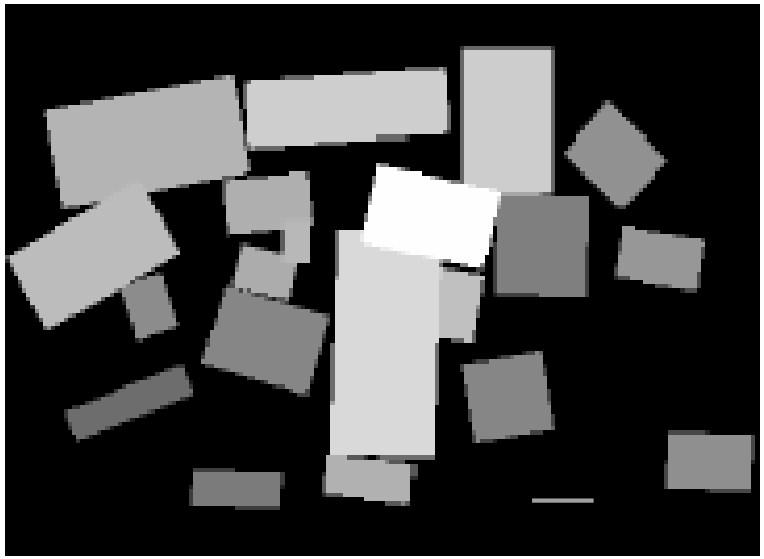

Bottom view

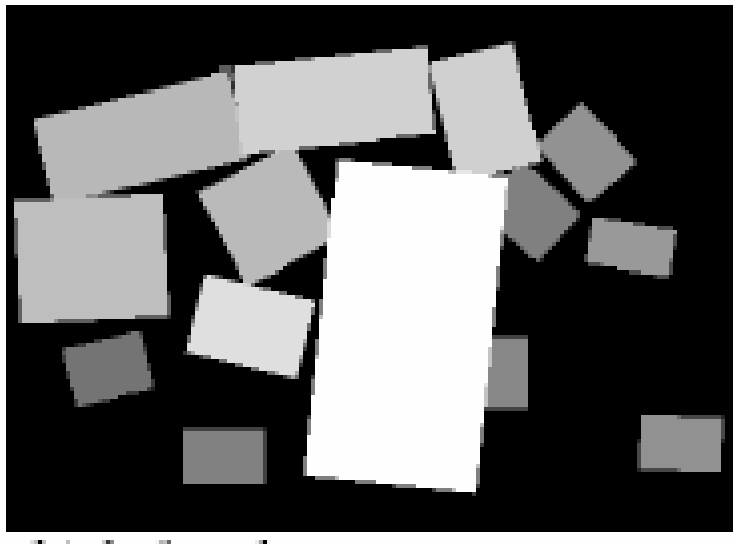

Left &Bottom

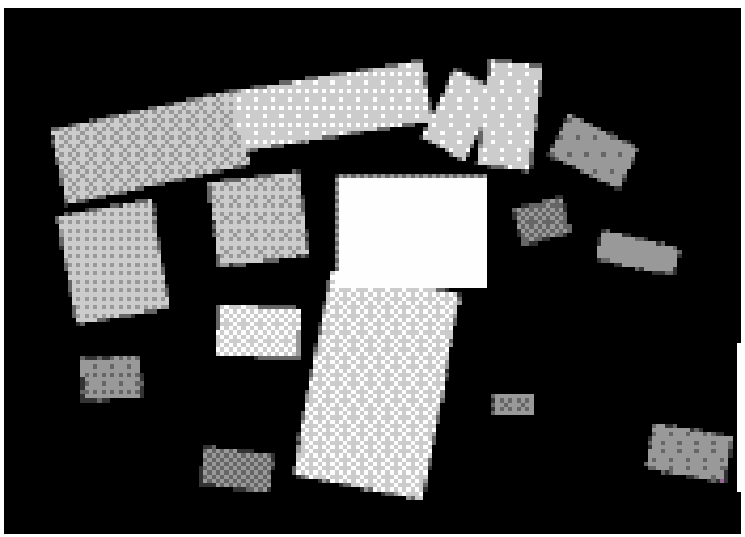

Left+Right+Bottom

Resulting Minimum Bounding Rectangles fit to point clouds detected automatically from maximum combined height map for different view combinations.

area 200 m x 150 m

Leberl F. W., Regine Bolter, From Multiple View Interferometric Radar to Building Models, Proc. EUSAR 2002

Quellenangabe

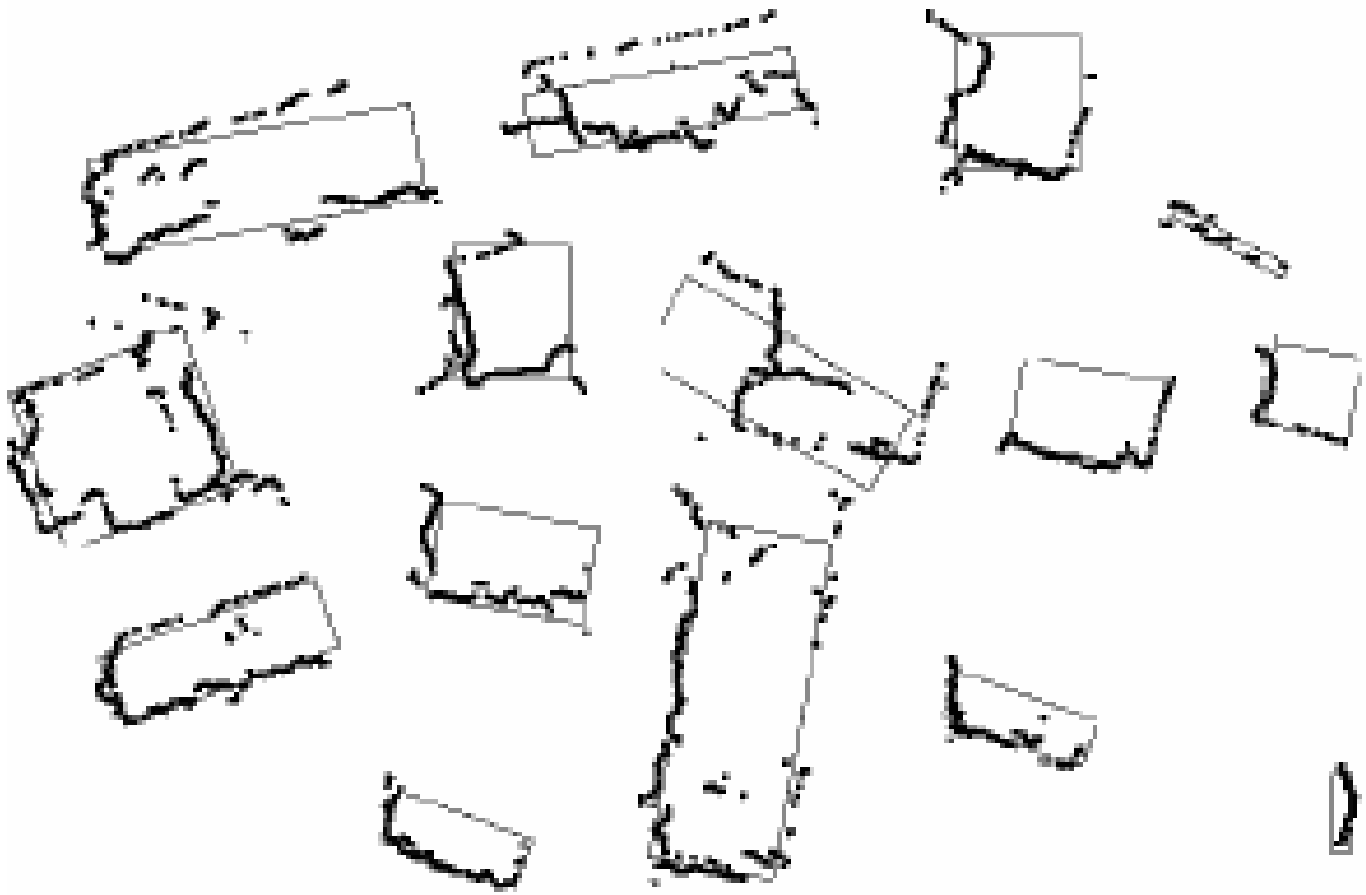

Footprints from shadows, reconstructed from two perpendicular views, right + top Overlaid are the computed optimum rectangles to fit the Point clouds.The area covers approximately 200 m x 150

Leberl F. W., Regine Bolter, From Multiple View Interferometric Radar to Building Models, Proc. EUSAR 2002

Quellenangabe

View Combination	Area Error (RMS)	Height Error (RMS)	detected Buildings
Bottom	± 205 m^2	± 2,1 m	21
Left + Right	± 276 m^2	± 2,6 m	12
Left + Bottom	± 422 m^2	± 1,6 m	14
Left +Right + Bottom	± 207 m^2	± 1,4 m	16
Left + Right +Top + Bottom	± 120 m^2	± 1,4 m	15

Resulting rms error of area & maximum height, result of applying the automated building detection algorithms to different view combinations. "Maximum height" is used to avoid the confusion resulting from sloping roofs. Leberl F. W., Regine Bolter, From Multiple View Interferometric Radar to Building Models, Proc. EUSAR 2002

Quellenangabe

Multiple View InSAR Data

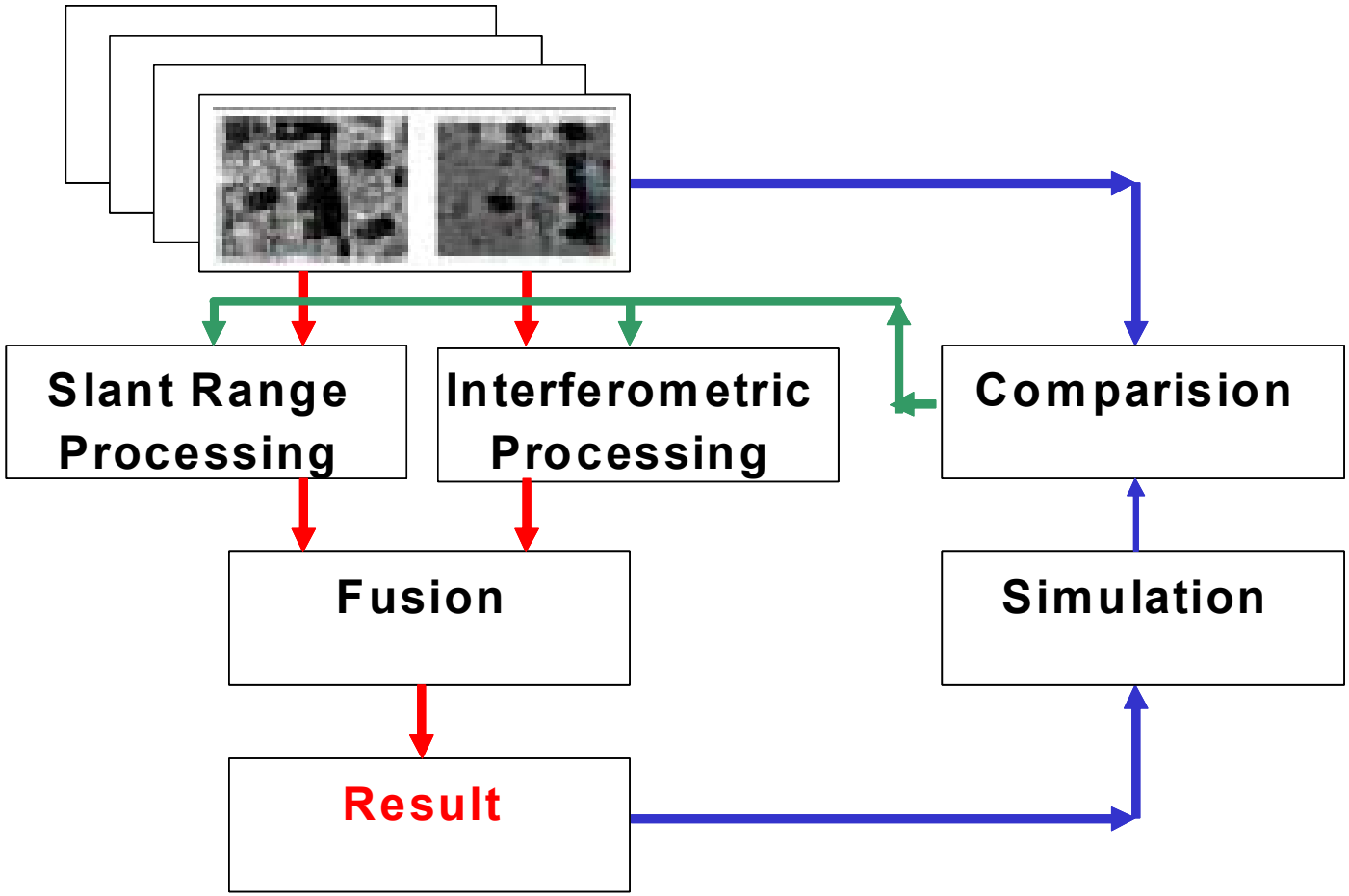

Procedure for the extraction of building models from a combination of SAR images and associated interferometric data [6]

R. Bolter, F. Leberl [2000]: „Phenomenology-Based and Interferometry-Guided Building Reconstruction from Multiple SAR Images“, Proc. EUSAR 2000, München, Germany, pp. 687-690

Quellenangabe

Traffic Monitoring

Velocity Measurements with Interferometric SAR

Ambigous Determination of Pixel Velocity

Azimuth Displacement:

$$V_{ve} = 3{,}6\, F_{gr} \left(\frac{V_{ae}\, x}{r_0} + n\, \frac{PRF\, \lambda}{2} \right)$$

Along Track Interferometry:

$$V_{ve} = -\frac{V_{ae}\, \lambda}{4\pi B} \left(\Phi + n 2\pi \right)$$

B: ATI Baseline; F_{gr}: Slant to Ground Range Factor: n: Ambiguity Number; PRF:Pulse Repetition Frequency; r_0: Slant Range Distance; x: Doppler Displacement; V_{ve}: vehicle velocity; V_{ae}: aercraft velocity;

λ: wavelength; Φ: Measured ATI Phase; 3.6:Conversion Factor m/s to km/h;

Quellenangabe

Airborne Moving Target Indication

Amplitude SAR Image

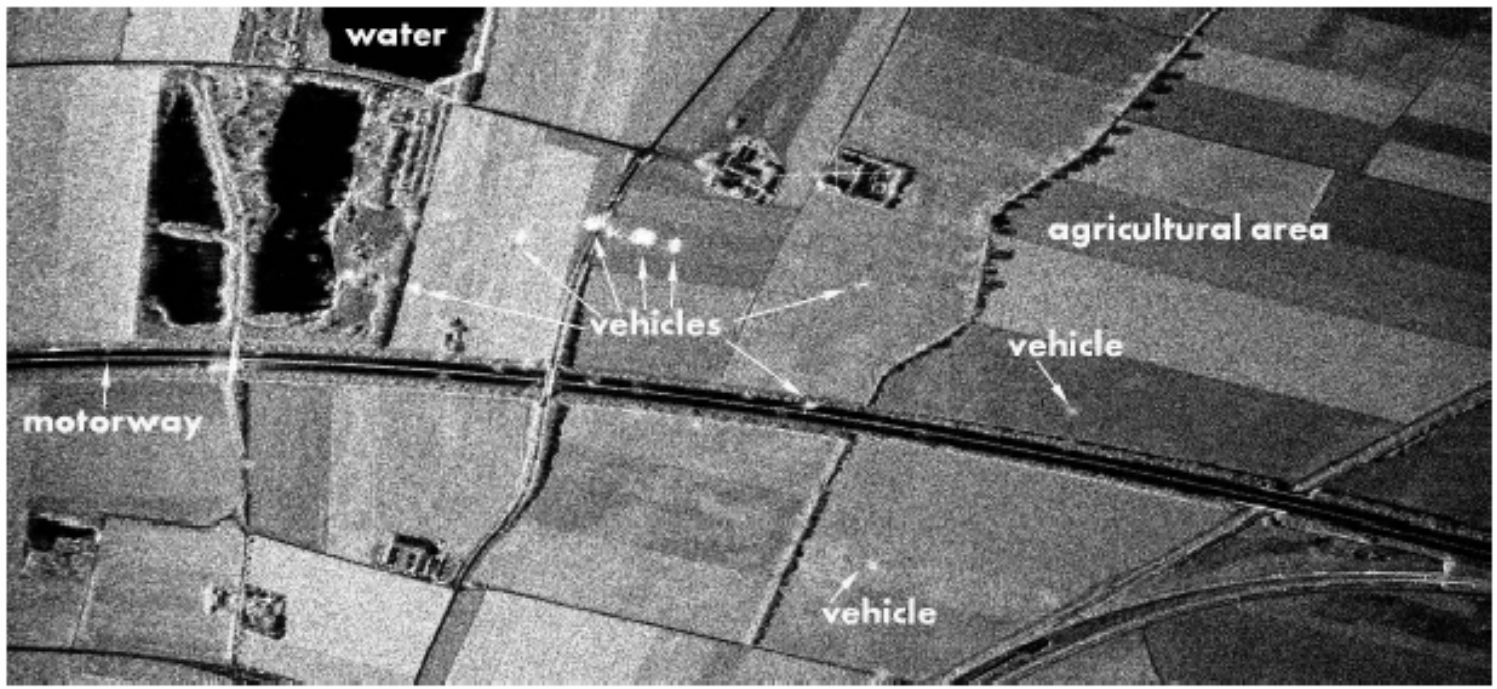

Motorway A 92 between Munich City and Munich Airport: **not all** vehicles are visible

Courtesy Joao Moreira, MFFU Summerschool 2001

Along-Track Interferometric Phase Image

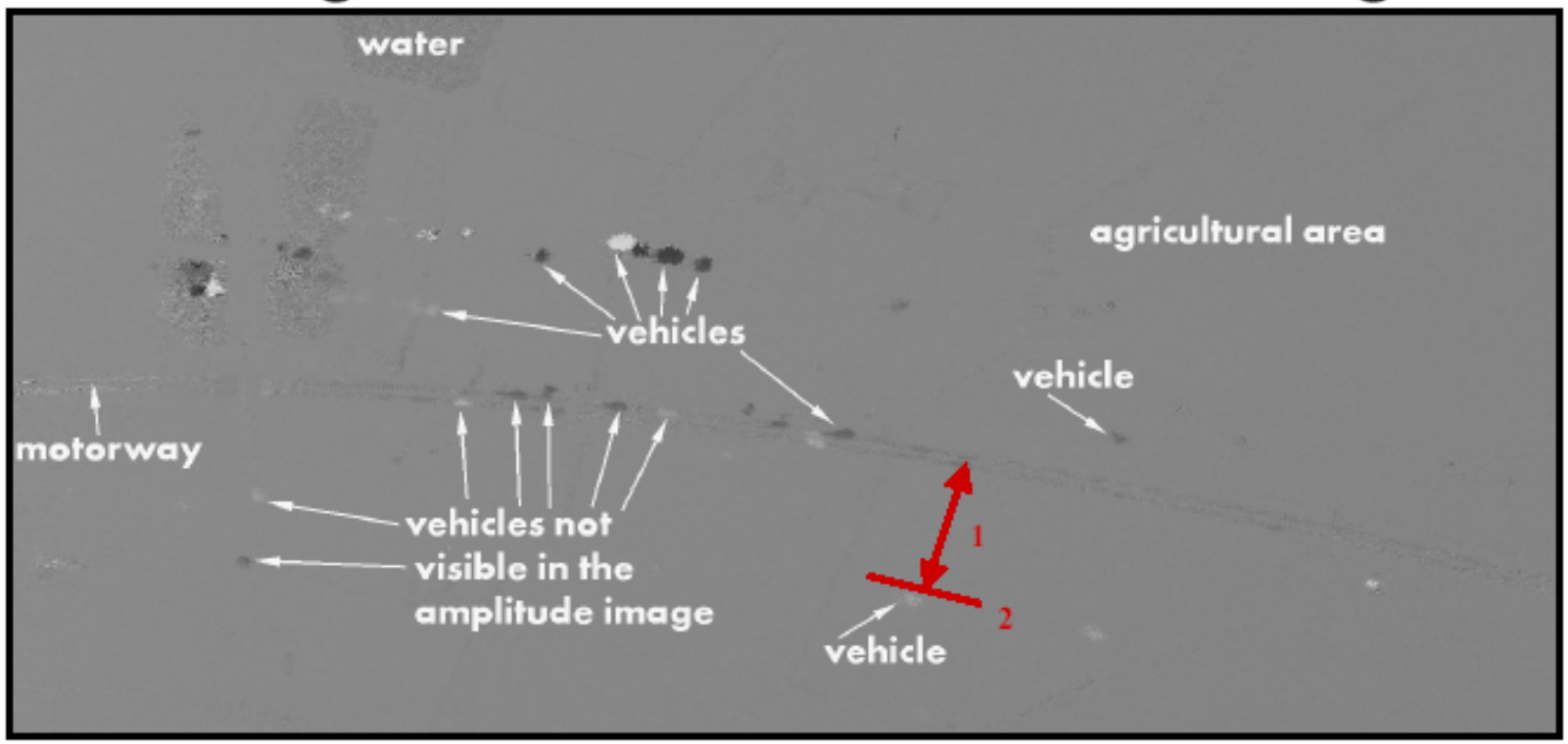

Motorway A2 between Munich City and Munich Airport: **all** vehicles are visible

1 Azimuth Displacement

2 ATI

Courtesy Joao Moreira, MFFU Summerschool 2001

Determination of the Car Direction from the Sub-Look Images

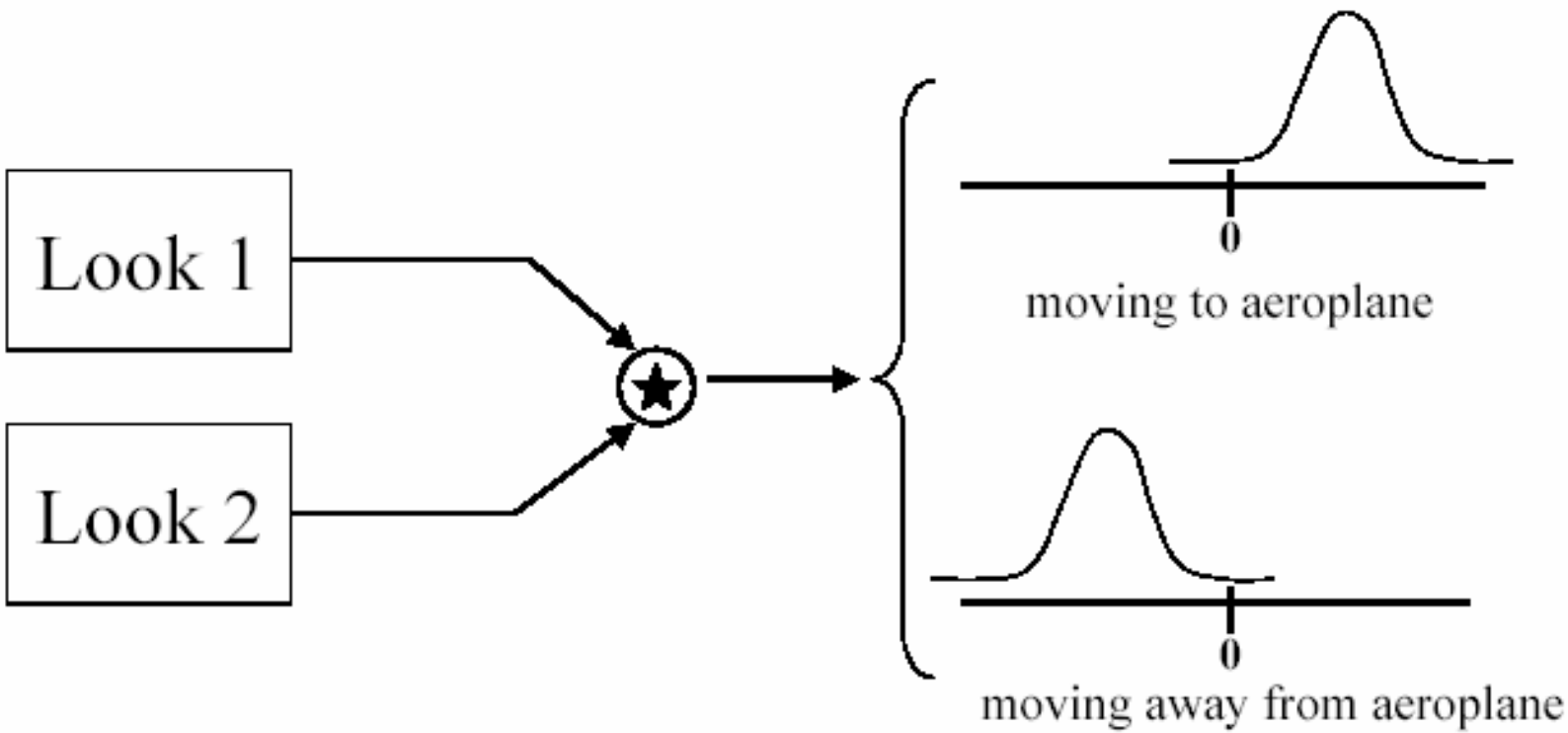

Courtesy Joao Moreira, MFFU Summerschool 2001

Sub-Look Images

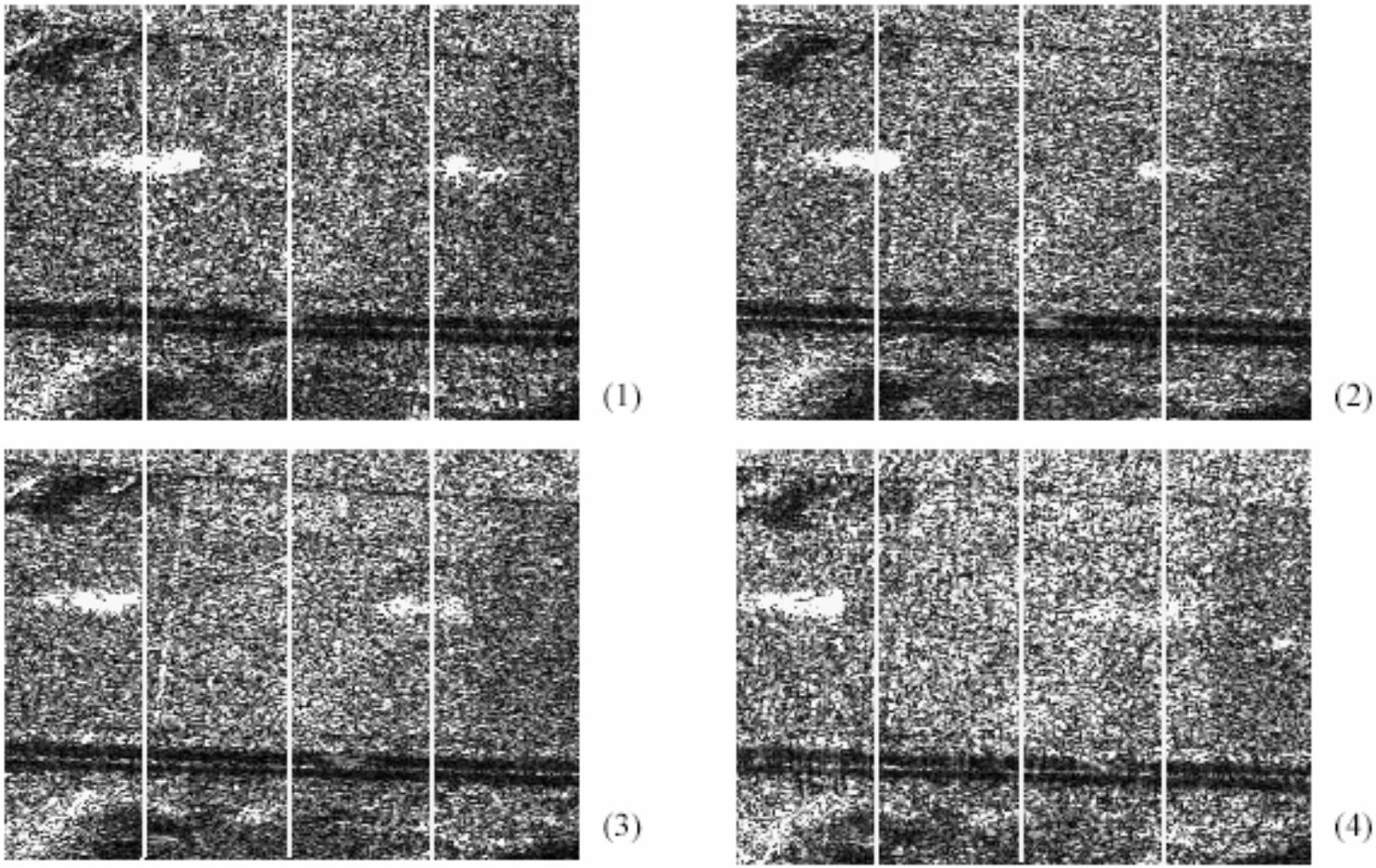

Courtesy Joao Moreira, MFFU Summerschool 2001

Acquisition of the Motorway

Traffic situation on the motorway A92 11. Nov. 1999 - 08:57:31 h

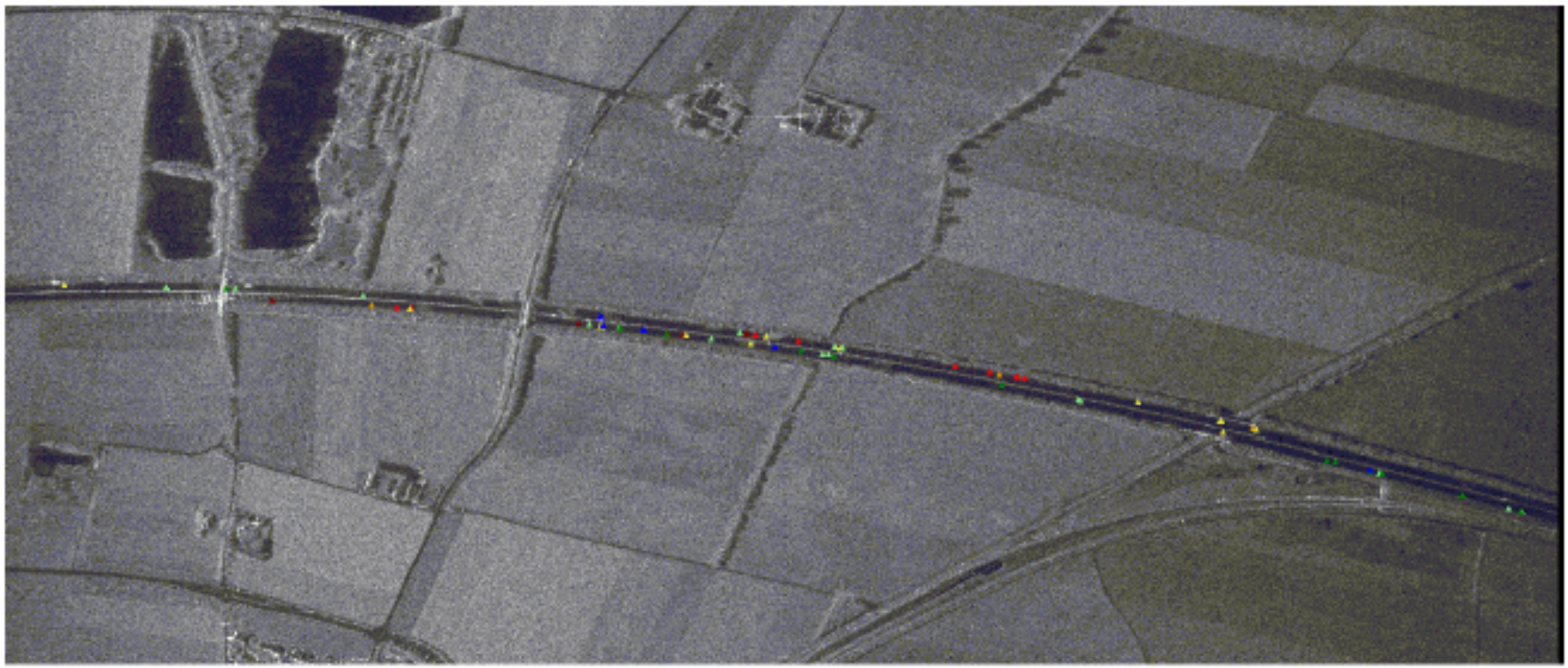

60 - 79 km/h
80 - 99
100 - 119
120 - 139
140 - 159
160 - 179
180 - 200

Motorway A92 between Munich City and Munich Airport

Quellenangabe

AEROSENSING RADAR-SYSTEME

Courtesy Joao Moreira, MFFU Summerschool 2001

Traffic Flow into town/ leaving town

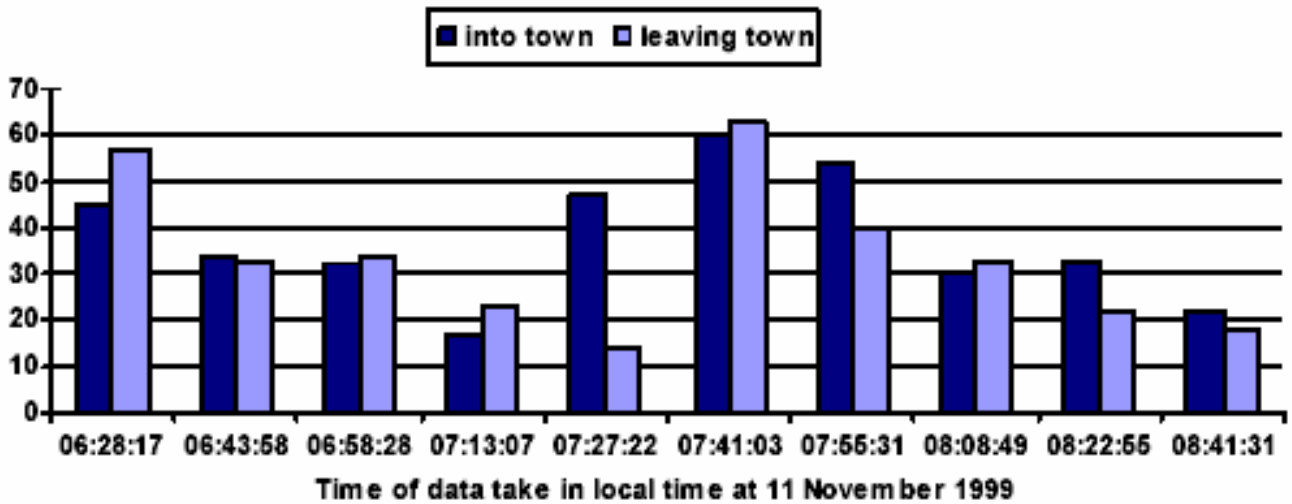

Measurements at Rosenheimer Straße, Munich

Courtesy Joao Moreira, MFFU Summerschool 2001

Moving and Not Moving Vehicles

(parking cars are excluded)

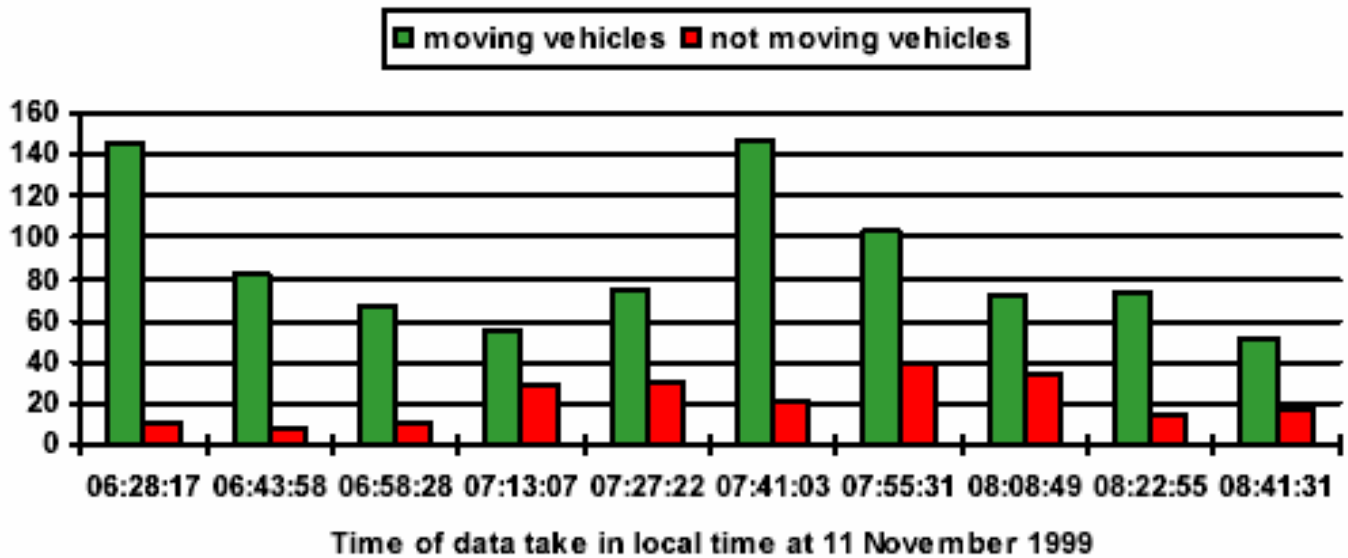

Measurements at Rosenheimer Straße, Munich

Quellenangabe

AEROSENSING RADAR-SYSTEME

Courtesy Joao Moreira, MFFU Summerschool 2001

Space-borne Moving Target Indication with SRTM

Along Track Interferometry Capability

Due to Antenna Displacement

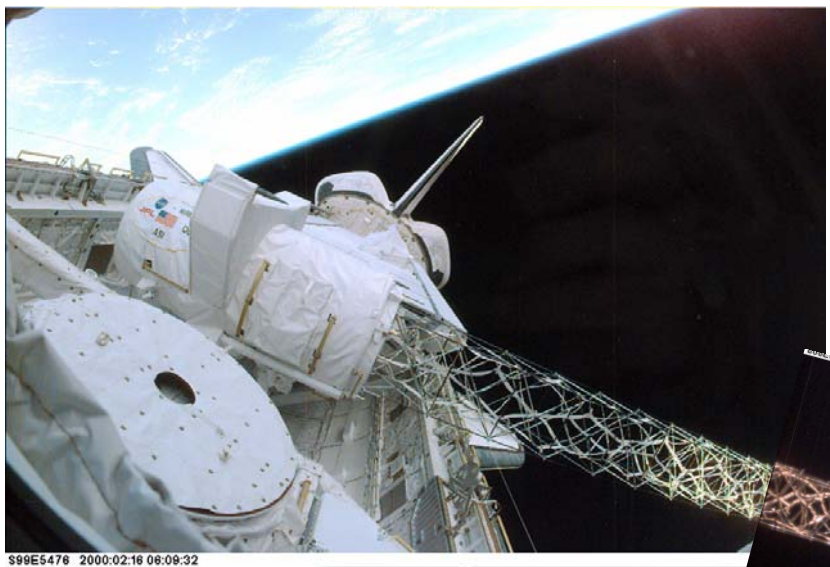

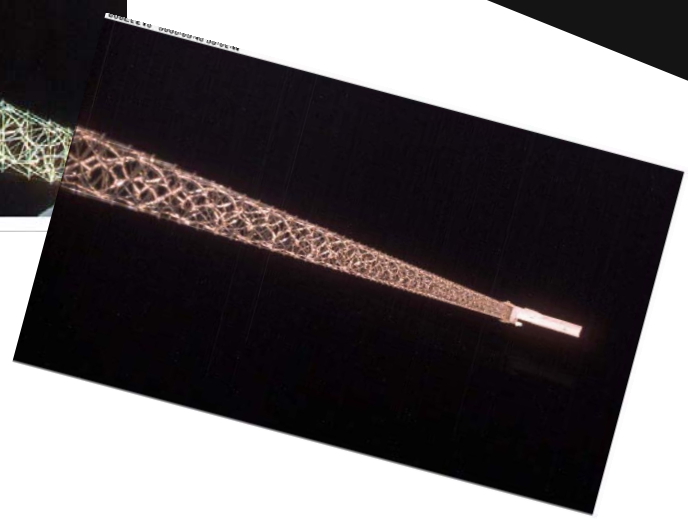

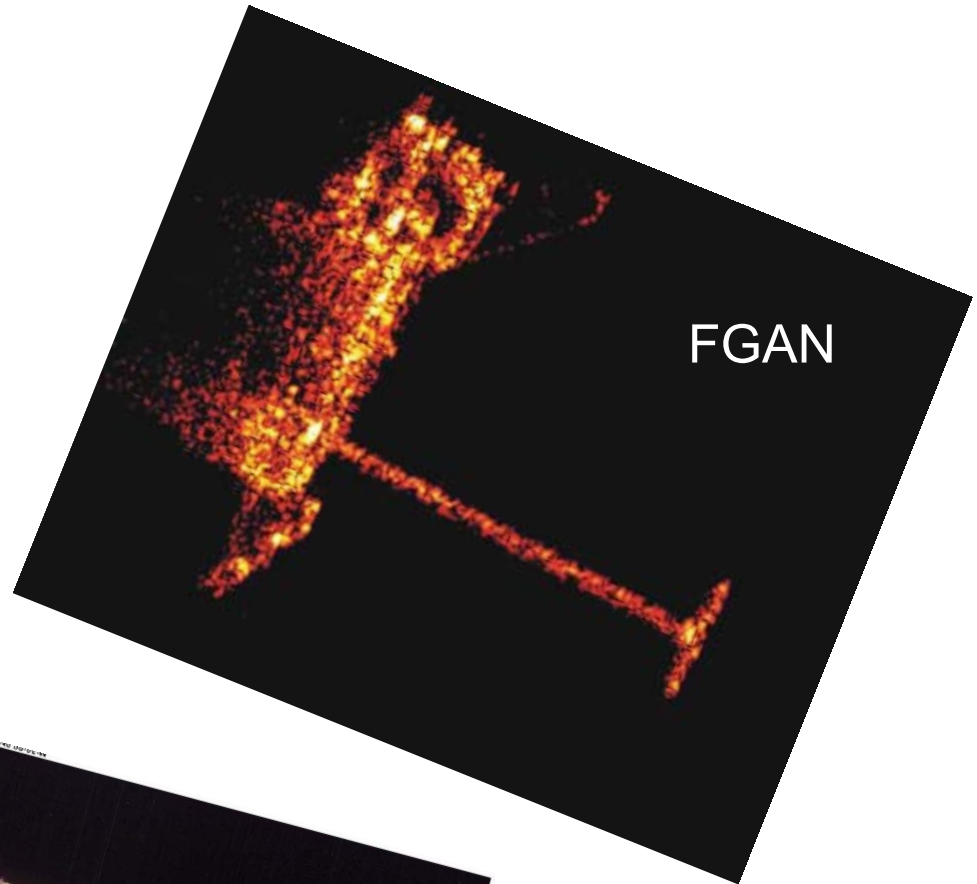

Quellenangabe

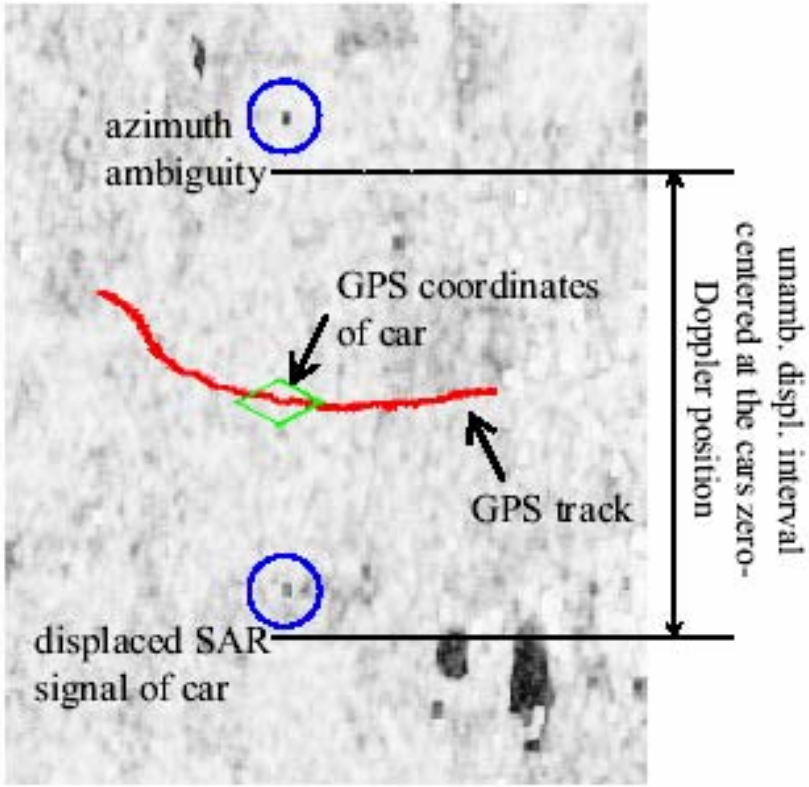

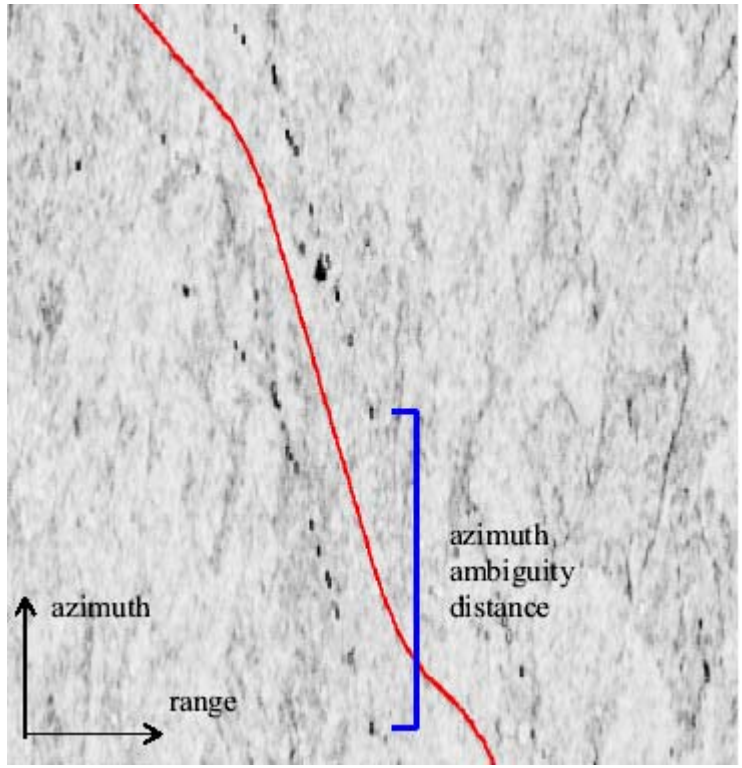

Coherence loss indicates the presence of a moving target. The larger low coherent areas are Lakes

Coherence map featuring a 3 km long section of the Autobahn Munich – Nuremberg. The black dots are cars displaced from the red road due to their velocities

Quellenangabe

[Breit et. al. , Traffic Momitioring using SRTM, Proc. IGARSS 2003]

Results of the Validation Experiment Comparing 3 Measurement Methods

InSAR data evaluation	
Velocities resulting from measured azimuth displacement (130.6 pixel)	
Radial Velocity from Displacement	37,9 km/h
Ground Velocity from Displacement	47,1 km/h
Velocities resulting from ATI Phase (127°)	
Radial Velocity from ATI Phase	42,2 km/h
Ground Velocity from ATI Phase	52,5 km/h
Velocity resulting from GPS Measurement	
Ground Velocity	48.33 km/h

Quellenangabe

MTI- Interferometry, SRTM/X-SAR (Bamler, DLR)

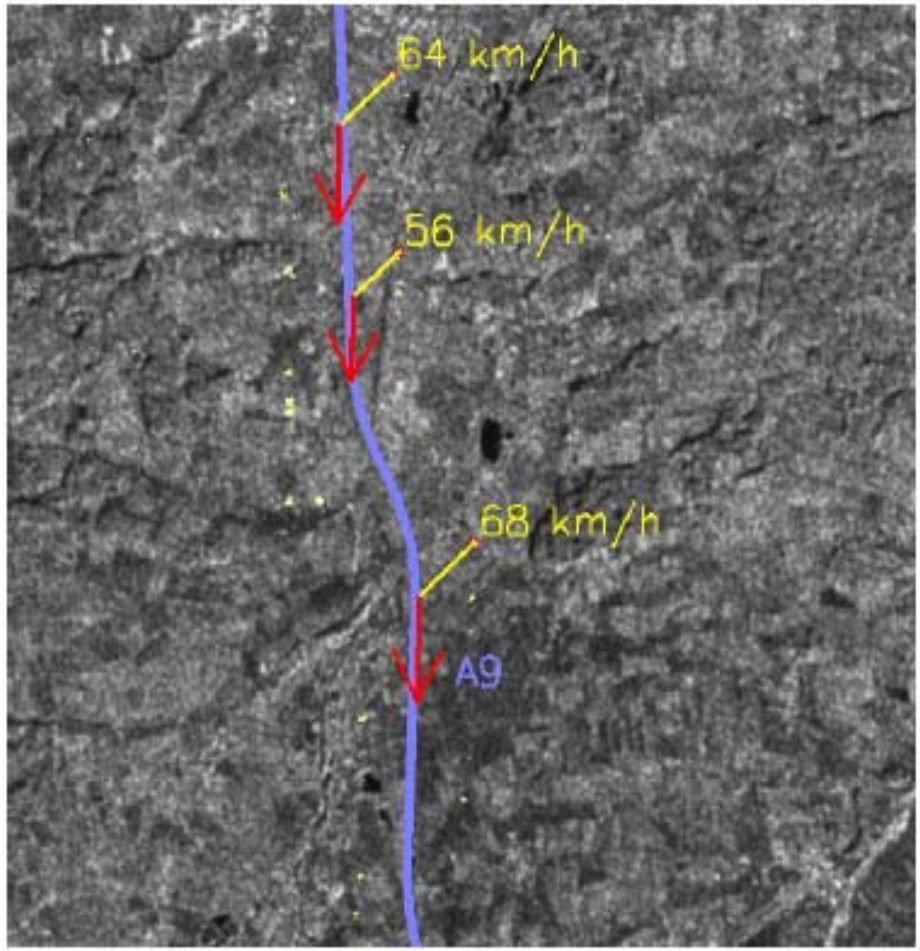

Left: Motorway A9, Munich – Nuremberg, Germany, arrow: SRTM track.
Right: SRTM/X-SAR image, motorway blue, red arrows vehicles with their velocities (yellow)

Quellenangabe

Ocean Current Measurements with SRTM Along Track Interferometry

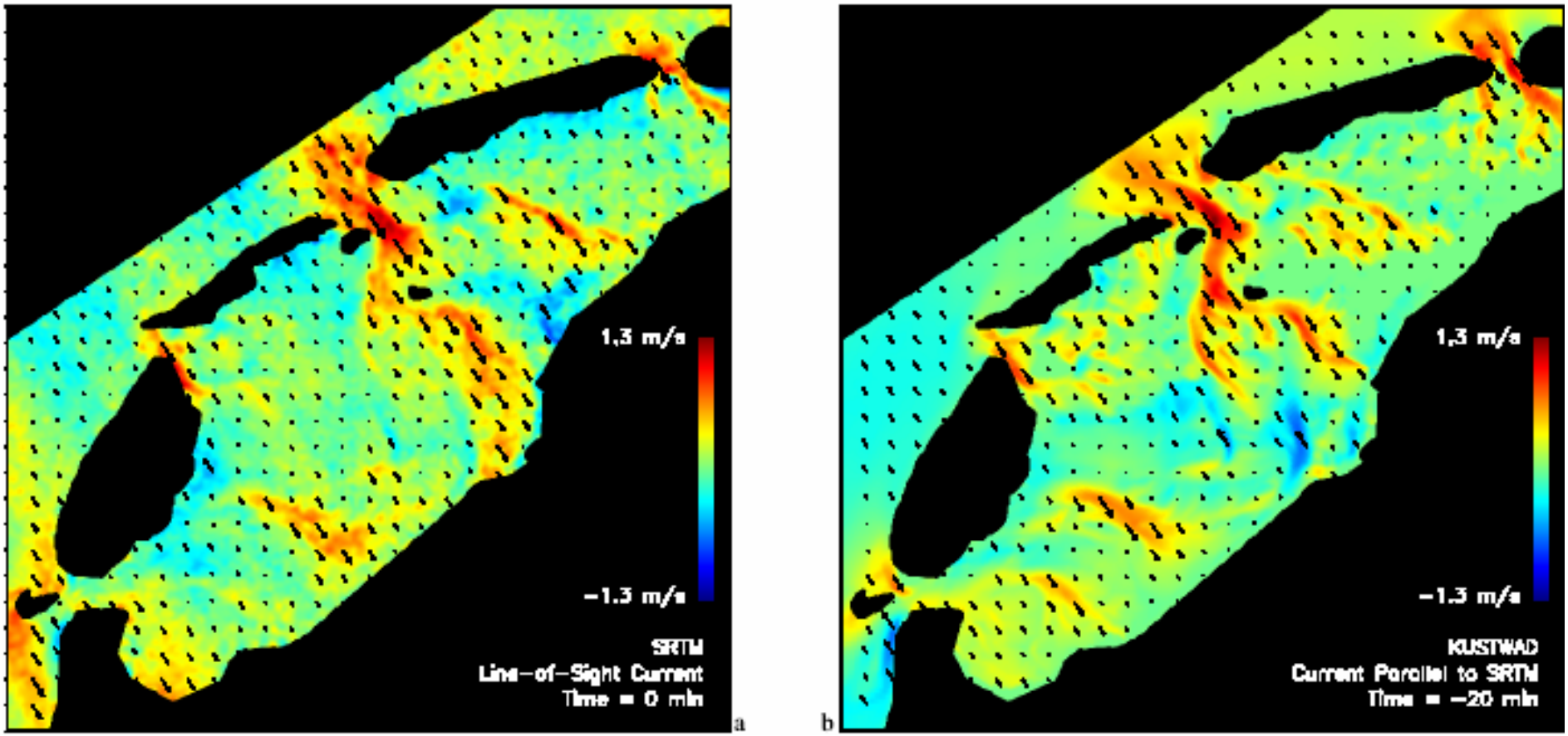

Line-of-sight current field derived from the SRTM data (left) & obtained from KUSTWALD for the tidal phase 20 minutes before SRTM overpass (right); grid resolution is 100 m × 100 m; data points with valid currents from SRTM and KUSTWAD are shown only.

Quellenangabe

Romeiser et. al. Validation of SRTM-Derived Surface Currents IEEE Proc. IGARSS 03,

Scatter diagram showing the distribution of SRTM-derived vs. KUSTWAD-derived current components in the SRTM look direction, as well as corresponding statistical quantities, for the tidal phase 20 minutes before the SRTM overpass.

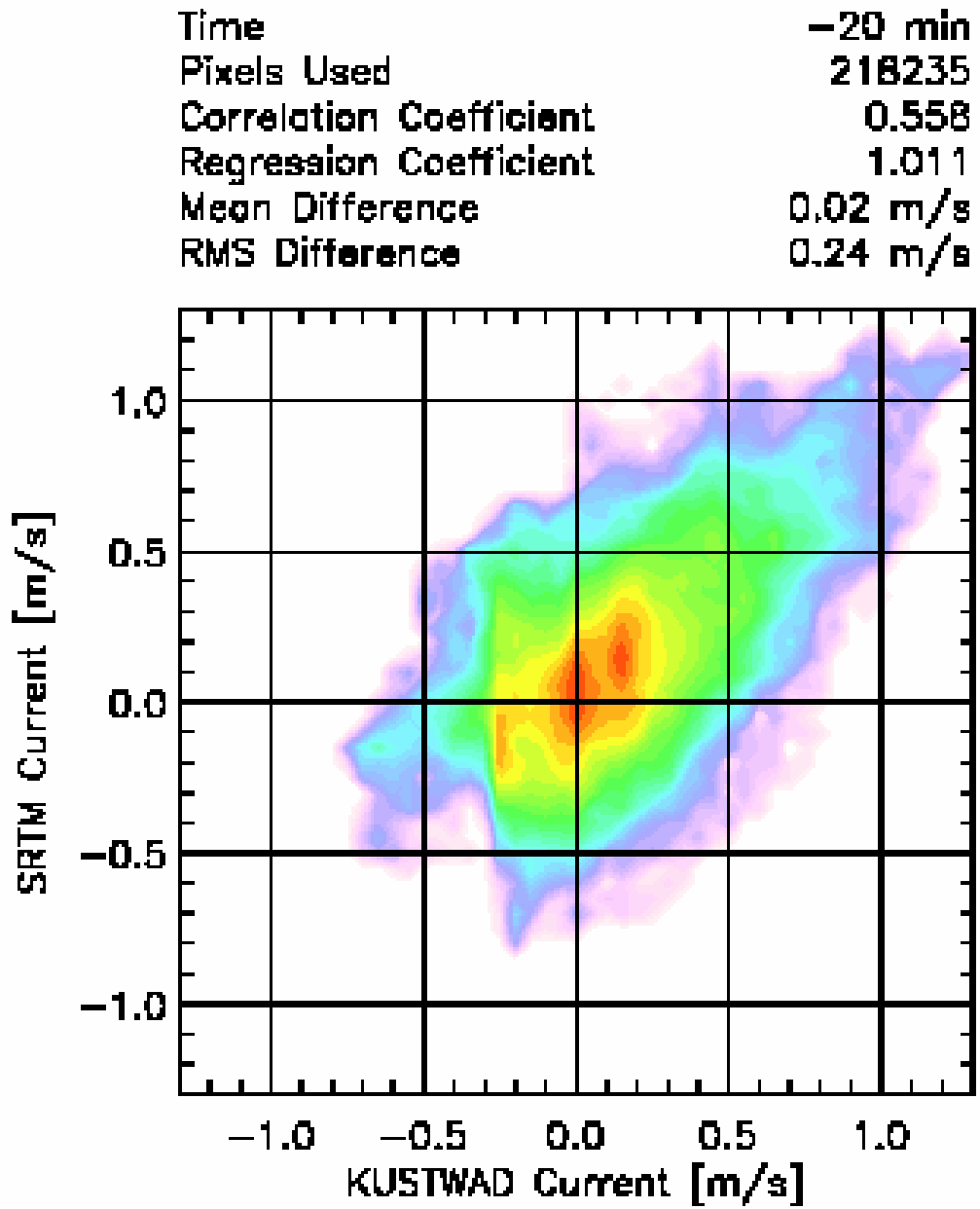

Romeiser et. al. Validation of SRTM-Derived Surface Currents IEEE Proc. IGARSS 03,

Quellenangabe

Mining Induced Subsidence by means of Differential SAR- & Permanent Scattering Interferometry

Quellenangabe

Determination of Subsidence Effect caused by Ground Water Withdrawal in a Brown Coal Mining Area with D - InSAR using Permanent Scatterers as Reference Points.

Goal

Clarify Correlation between Ground Water Withdrawal, Tectonics & Subsidence on Surface by means of both Differential SAR Interferometry & Permanent Scatterer Technique

D – InSAR: 28 ERS-1 Images registered to the same Master Image

PSI: 39 Interferograms from May 1995 to December 2000.

- Perpendicular Baselines: 23 m --- 500 m (--- 1158m).
- 17 D-InSAR Interferograms showed Concentric, nearly Elliptic Fringes, each corresponding to 28 mm Line of Sight Movement.
- For PSI 11.000 Permanent Scatterers were identified & within a reference network selected for more point wise information
- From May 1995 to December 2000 the area affected by groundwater withdrawal sank continuously with 5 cm/year.

Quellenangabe

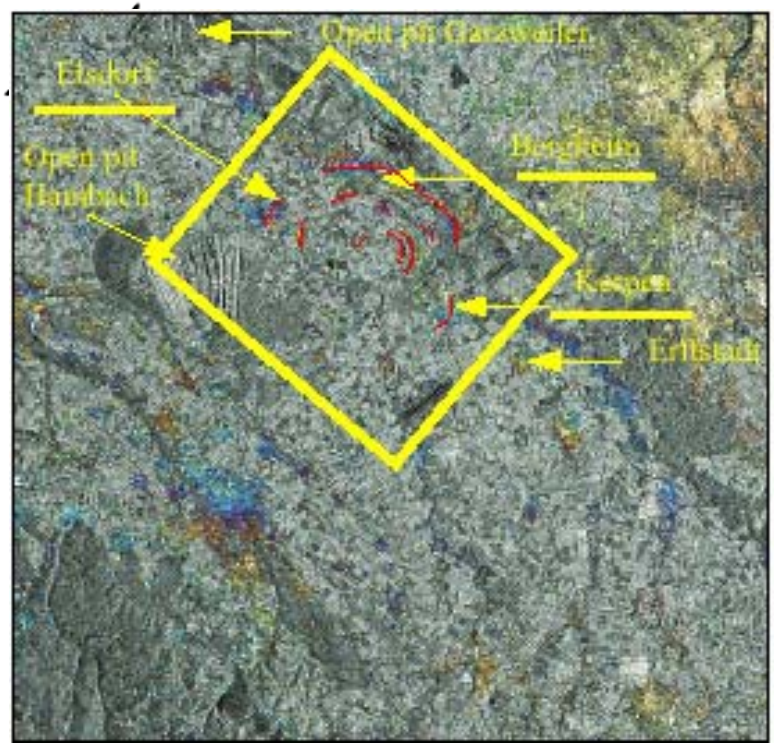

Differential Interferogram with Amplitude Overlay

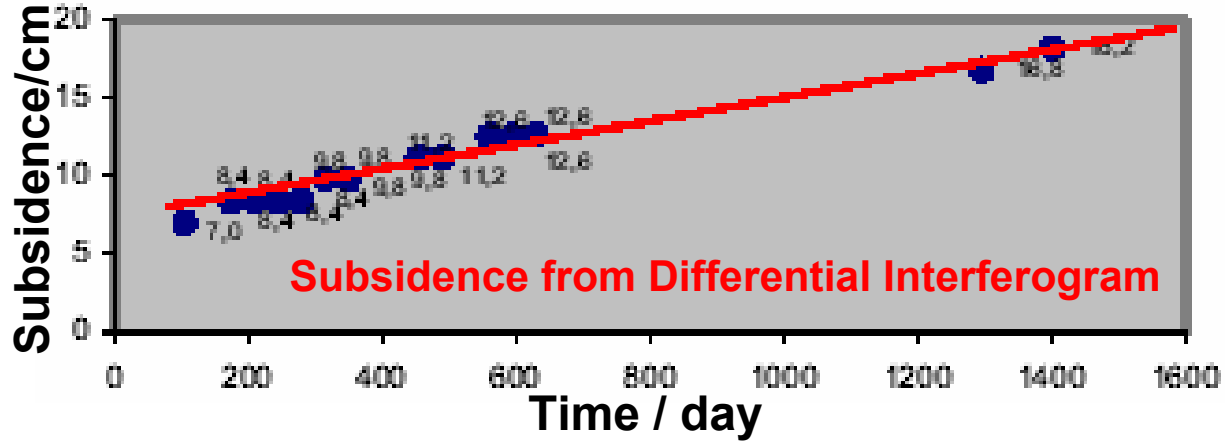

Results: Both techniques lead to the same subsidence rates of about 5 cm/year. Even over a time span of 1401 days reliable results were achieved with both methods. The estimated values could be verified by ground measurements of the land surveying office NRB, Germany.

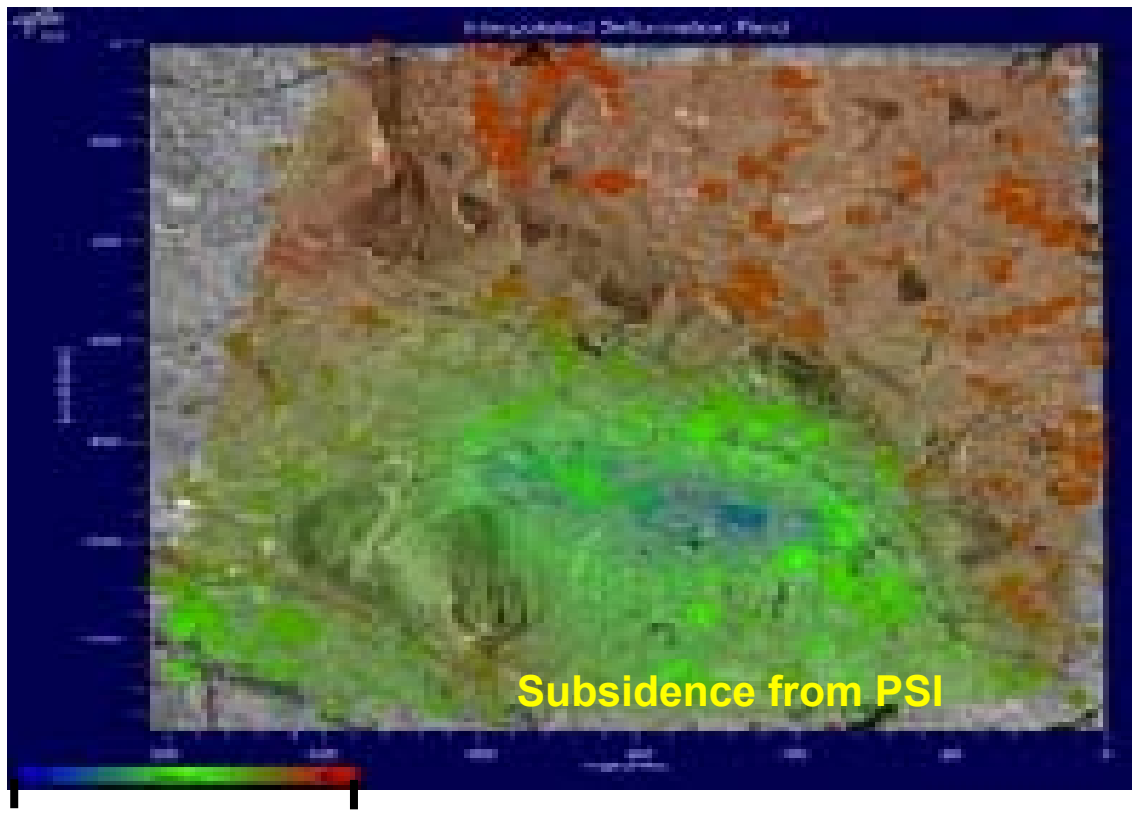

+4 cm **- 4 cm**

Quellenangabe

Kircher et. al. Proc.Remote Sensing observations of mining induced subsidence, IGARSS 2003,

Soil Moisture & Biomass Estimation using Polarimetric Scattering Theory

User Requirements

	BIOMASS	SOIL MOISTURE CONTENT
Spatial Resolution	1/2 ha = 5000m^2	70x70m
Temporal Resolution	4 Years	
	Average Tree Height Change: 3m -- 4 m per Year Differential Height Accuracy: 1 m	Seasonal observation > 2 per Year
Required Accuracy	Tree height estimation: 10% Mean forest height on Earth: 20 m Height Accuracy: 2 m	Volumetric Moisture 10% - 20 %

Quellenangabe

State of the Art for Soil Moisture Estimation

accuracy moisture content & surface roughness of <u>bare surfaces</u> :10 - 20%, moisture content ranging from 0 up to 40 [vol. %]

roughness scales up to ks < 1.

Uncertainties during measuring the surface parameters lead to inaccuracies.

Main Problem

Presence of Vegetation Cover Limits Algorithm Performance Drastically
Scattering Decomposition Techniques lead to Improvements but do not solve the problem

Possible Solutions

Dual-Frequency Polarimetry (for example: L- and P-band)
Combination of Mono- and Bi-Static Polarimetric Measurements
Combination of Polarimetric and Interferometric Measurements

Quellenangabe

Assumption: Surface Scatterer
Entropy H < 0.4 & α < 0.40°

$$[C] = \lambda_1 \vec{e}_1 \vec{e}_1^{\,+} + \lambda_2 \vec{e}_2 \vec{e}_2^{\,+} + \lambda_3 \vec{e}_3 \vec{e}_3^{\,+} = [C_1] + [C_2] + [C_3]$$

$$[C_i] = \vec{\mathbf{k}}_\mathbf{i} \vec{\mathbf{k}}_\mathbf{i}^{\,+} \quad \text{with} \quad \vec{\mathbf{k}}_\mathbf{i} = \lambda_\mathbf{i} \mathbf{e}_\mathbf{i} = [\mathrm{HH}_\mathbf{i}, \sqrt{2}HV_i, VV_i]$$

$[C_1]$ represents deterministic anisotropic surface scattering

$[C_2]$ & $[C_3]$ correspond to double-bounce and/or multiple scattering components respectively.

In this sense: $|HH_1|$, $|VV_1|$, and $|HV_1|$ values represent the scattering amplitudes corresponding to the surface scattering only.

The disturbing double-bounce (if present) and multiple scattering effects affecting the original |HH|, |VV|, and |HV| have been filtered out.

The Polarimetric Eigenvector Decomposition Technique
Covariance Matrix *[C]* & Scattering Vector $\vec{k}$

$$[C] = \left\langle \vec{k}\vec{k}^{+} \right\rangle = \begin{bmatrix} \langle |HH|^2 \rangle & \sqrt{2}\langle HHHV^* \rangle & \langle HHVV^* \rangle \\ \sqrt{2}\langle HVHH^* \rangle & 2\langle |HV|^2 \rangle & \sqrt{2}\langle HVVV^* \rangle \\ \langle VVHH^* \rangle & \sqrt{2}\langle VVHv^* \rangle & \langle |VV|^2 \rangle \end{bmatrix} \qquad \vec{\mathrm{k}} = [HH, \sqrt{2}\,HV, VV]^T$$

Decomposition of [C] leads to three 3 x 3 Independent Rank 1 Covariance Matrices [C_i]

$$[C] = \lambda_1 \vec{e}_1 \vec{e}_1^{+} + \lambda_2 \vec{e}_2 \vec{e}_2^{+} + \lambda_3 \vec{e}_3 \vec{e}_3^{+} = [C_1] + [C_2] + [C_3]$$

$$[C_i] = \vec{\mathrm{k}}_i \vec{\mathrm{k}}_i^{+} \quad \text{with} \quad \vec{\mathrm{k}}_i = \lambda_i \mathrm{e}_i = [\mathrm{HH}_i, \sqrt{2}HV_i, VV_i]$$

$\lambda_1 > \lambda_2 > \lambda_3$: real non negative eigenvalues of [C]; e_i (i = 1,2,3): eigenvectors.
[C_i] orthogonal & independent

Soil moisture Map: mv in Vol %

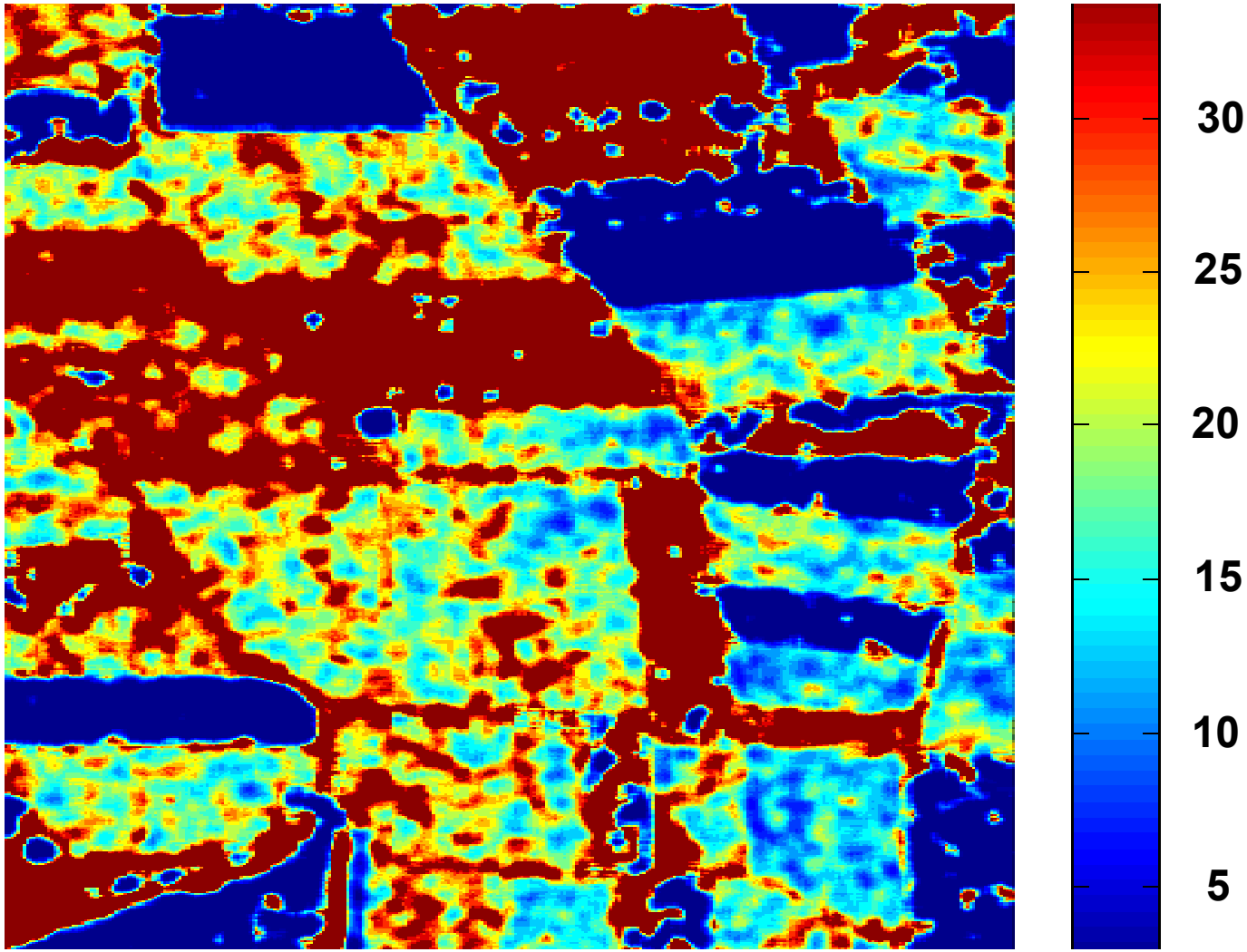

Quellenangabe

Hajnsek et. al., Terrain Correction for Quantitative Moisture and Roughness Retrieval… *Proc.IGARSS'00*,

Soil Surface Roughness Map *ks*

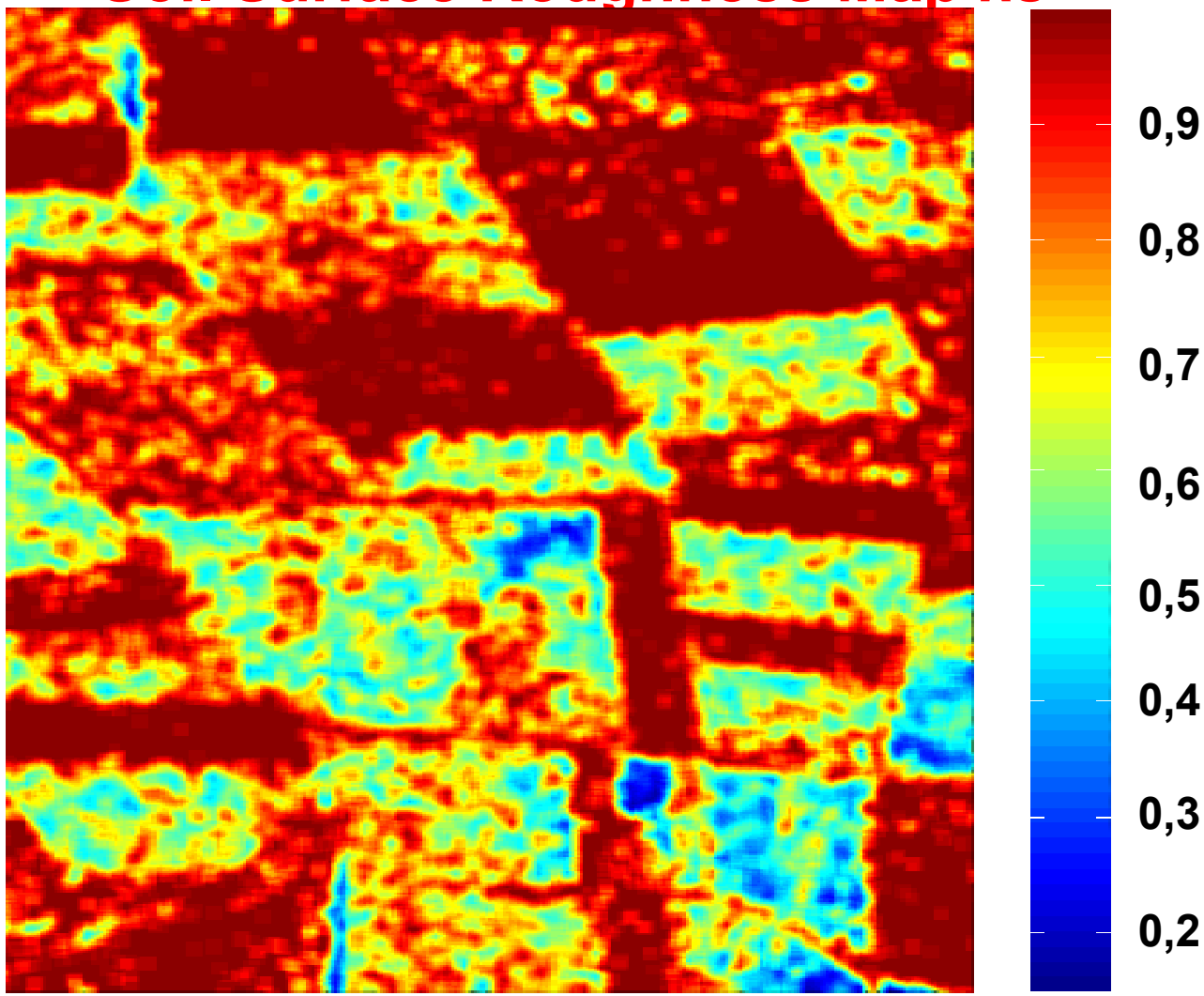

Quellenangabe

Hajnsek et. al., Terrain Correction for Quantitative Moisture and Roughness Retrieval… *Proc.IGARSS'00*,

Measured versus Estimated Soil Moisture

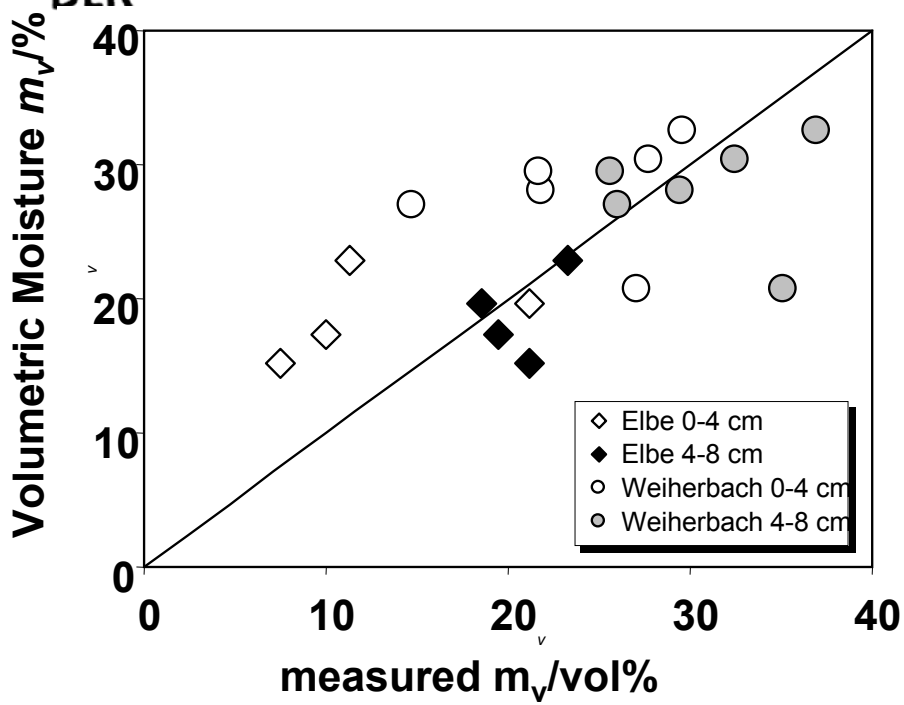

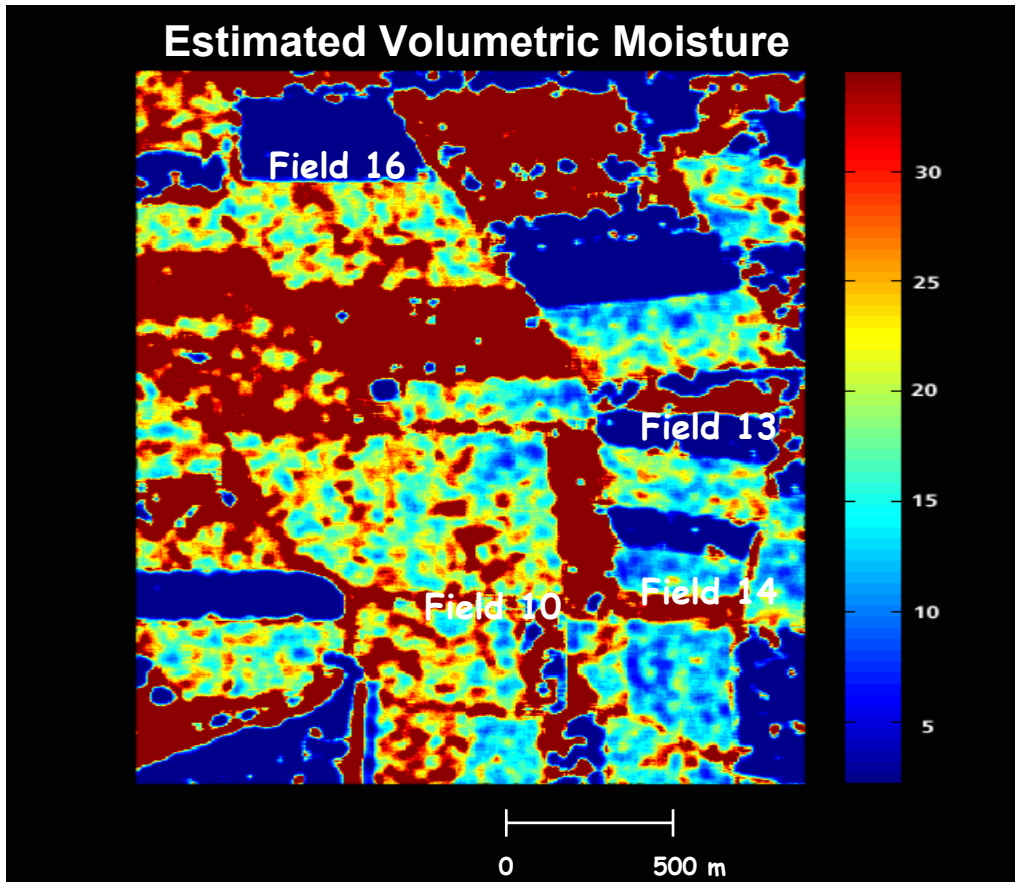

	0-4 cm	4-8 cm	corr.
Elbe RMS_{error}	8	3	0.7/0.8
Weih RMS_{error}	7	6	0.2/-

Quellenangabe

Hajnsek et. al., Terrain Correction for Quantitative Moisture and Roughness Retrieval… *Proc.IGARSS'00*,

Which is the Optimum Frequency Band ???

C-band

Pro:

Established Technology

Contra:

Limited Penetration Capability in Dense Vegetation

Temporal Decorrelation (repeat pass implementation)

ks range to small for a variety of natural surfaces

L-band

Pro:

Established Technology
Higher Penetration Capability
Wide Spectrum of Applications

ks range covers most natural surfaces

Contra:

Long Term Temporal Decorrelation (repeat pass implementation)

Open Question:

Does L-band see the ground in tropical forest???

P-band

Pro:

Approved Penetration Capability in Tropical Forest

Contra:

Spatial Resolution (Limited Bandwidth)

Non-Established Technology

Limited Application Spectrum

Interpretation of Coherence Maps
Results from SIR-C

Multifrequency Interferogram Magnitudes, Mt. Etna SIR-C

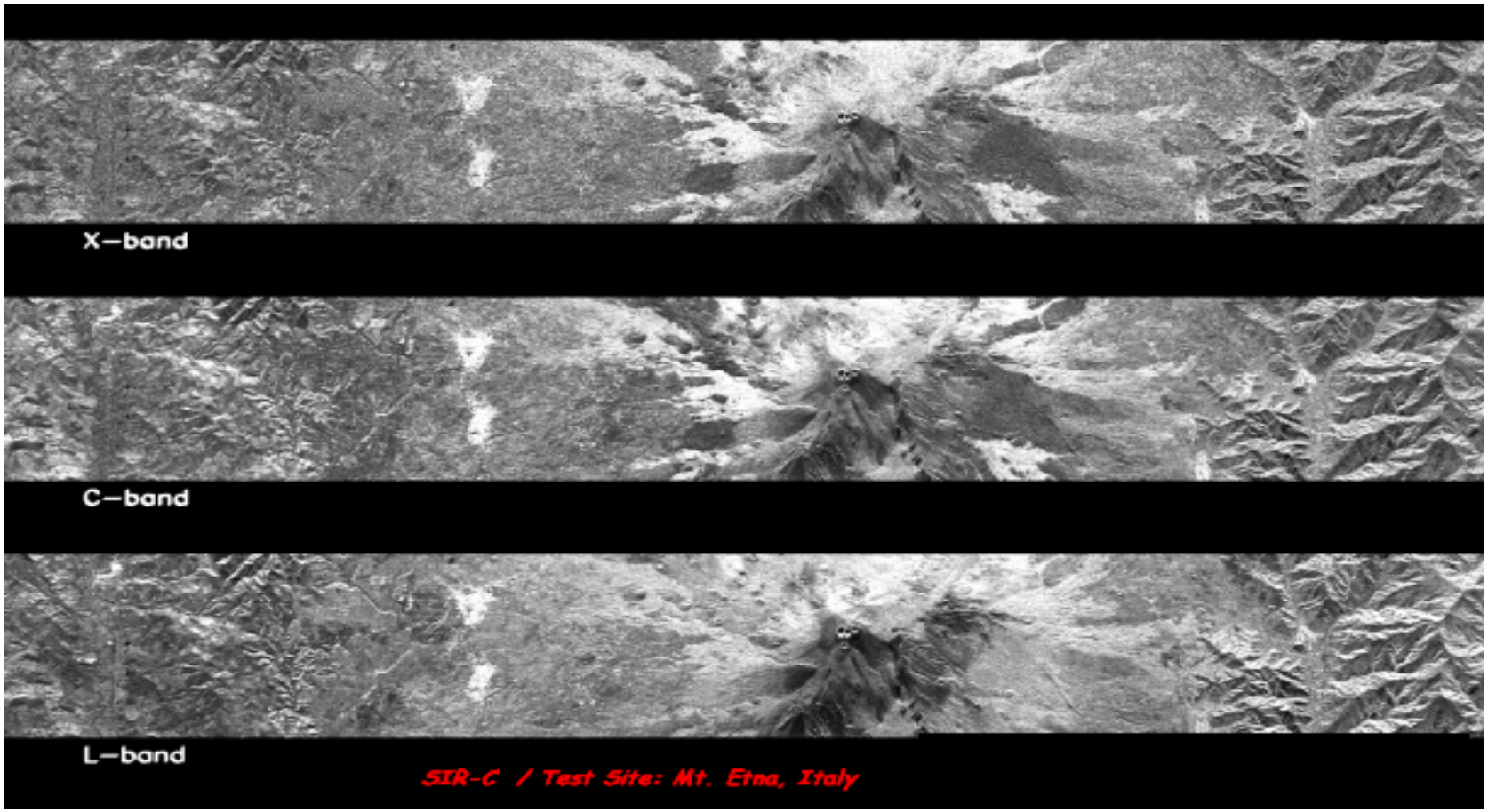

Co-registered slant range SAR images. Ground range: 66.8 km x 9 km
X-band:16000 pulses &1024 range bins, L- and C-band: 2048 range bins

Quellenangabe

Coregistered Interferogrammes with flat earth, Mt. Etna, SIR-C

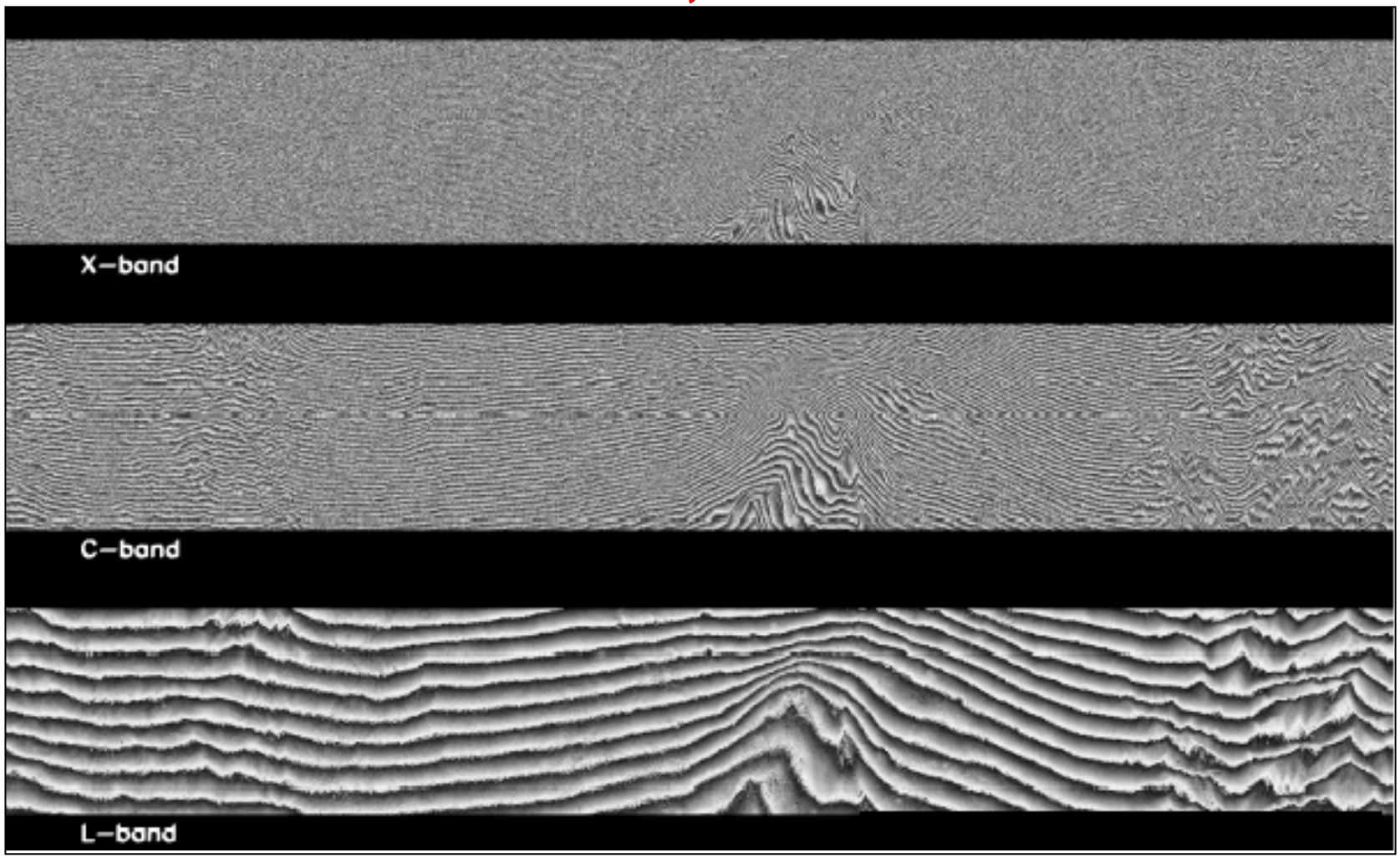

Coregistered Set of Interferogrammes

Quellenangabe

Coregistered Multifrequency Interferogrammes, Mt. Etna, after Flat Earth Removal

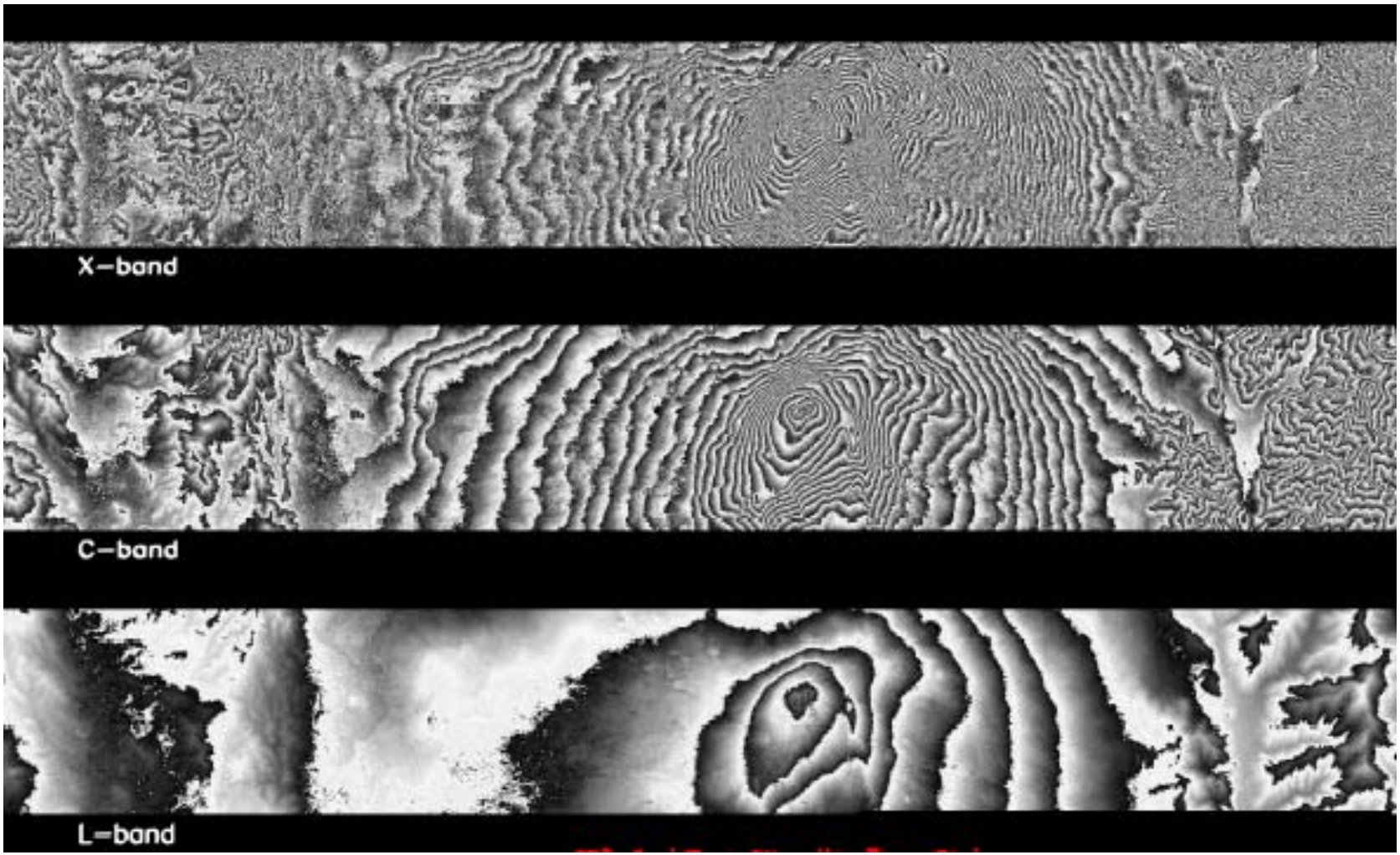

Ground range: 66.8 km x 9 km.

X-band:16000 pulses &1024 range bins, L- and C-band: 2048 range bins

Coregistered Coherence Maps, Mt. Etna, SIR-C

X-Band

C-Band

L-Band

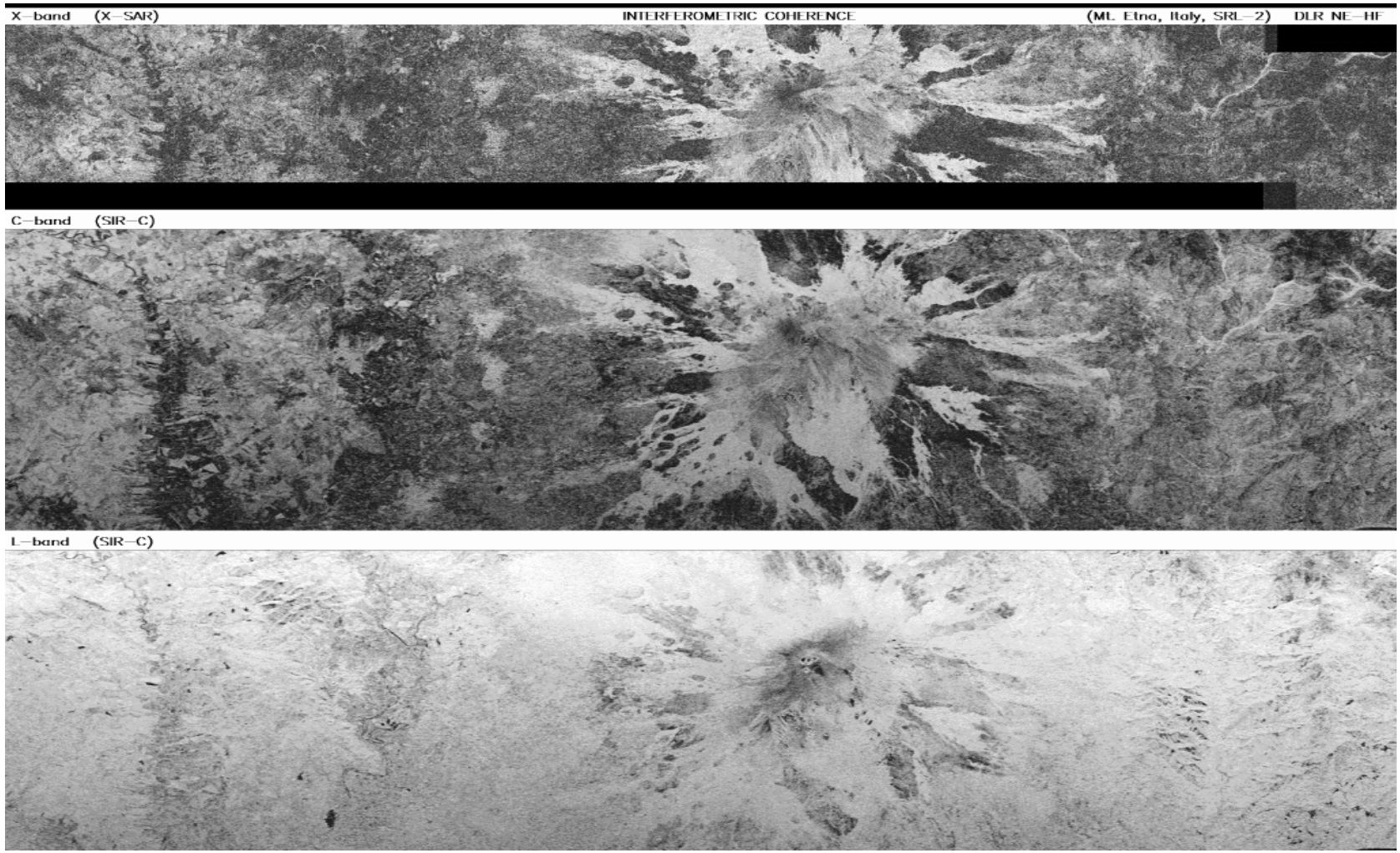

Ground range: 66.8 km x 9 km.

X-band:16000 pulses &1024 range bins, L- and C-band: 2048 range bins

Quellenangabe

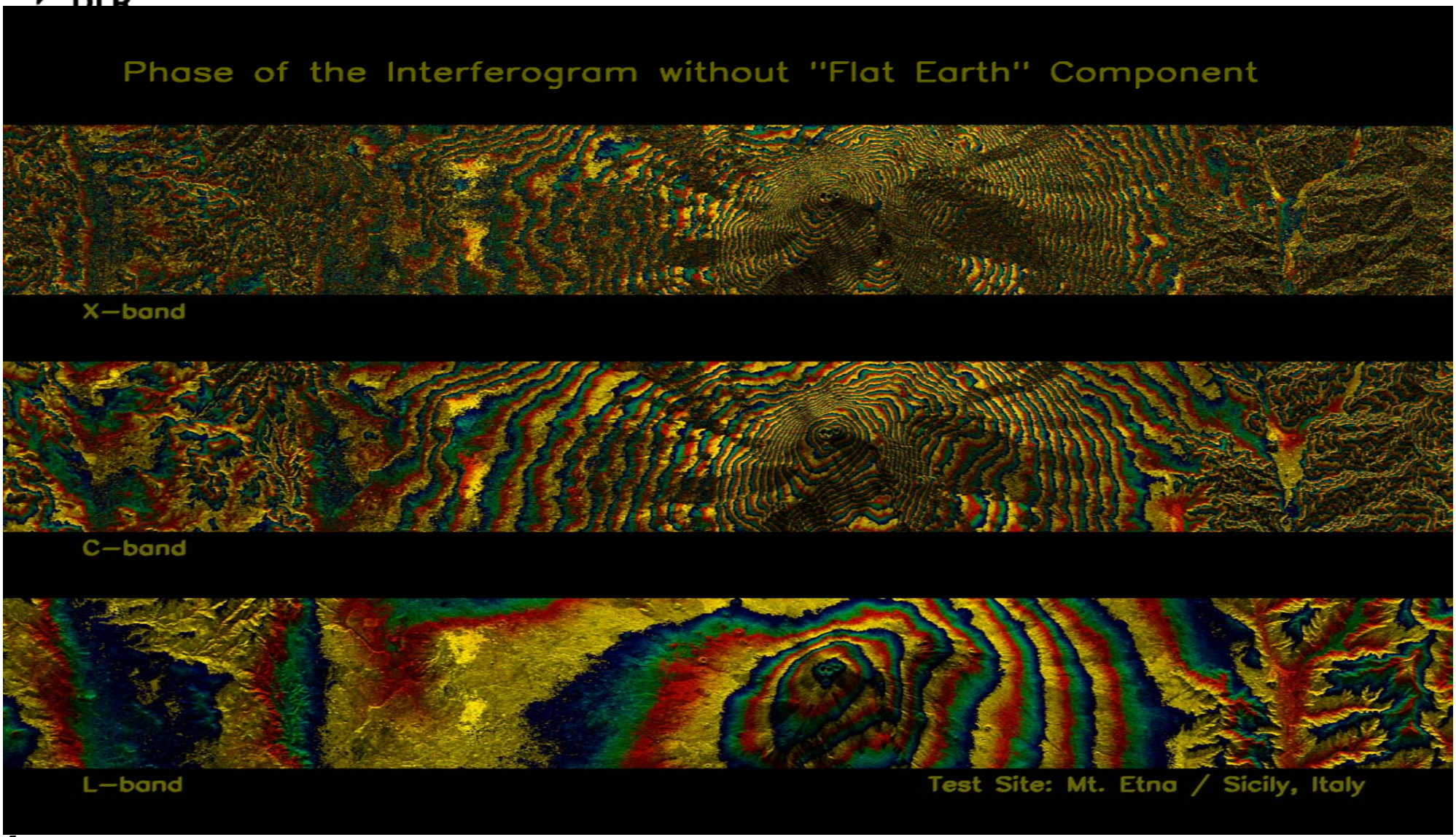
Phase of the Interferogram without "Flat Earth" Component
X–band
C–band
L–band
Test Site: Mt. Etna / Sicily, Italy

Quellena

Multifrequency Phase Unwrapping

Wrapped Phases with E_f

E_f: Scaled Flat Earth Funktion

Unwrapped Phases without E_f

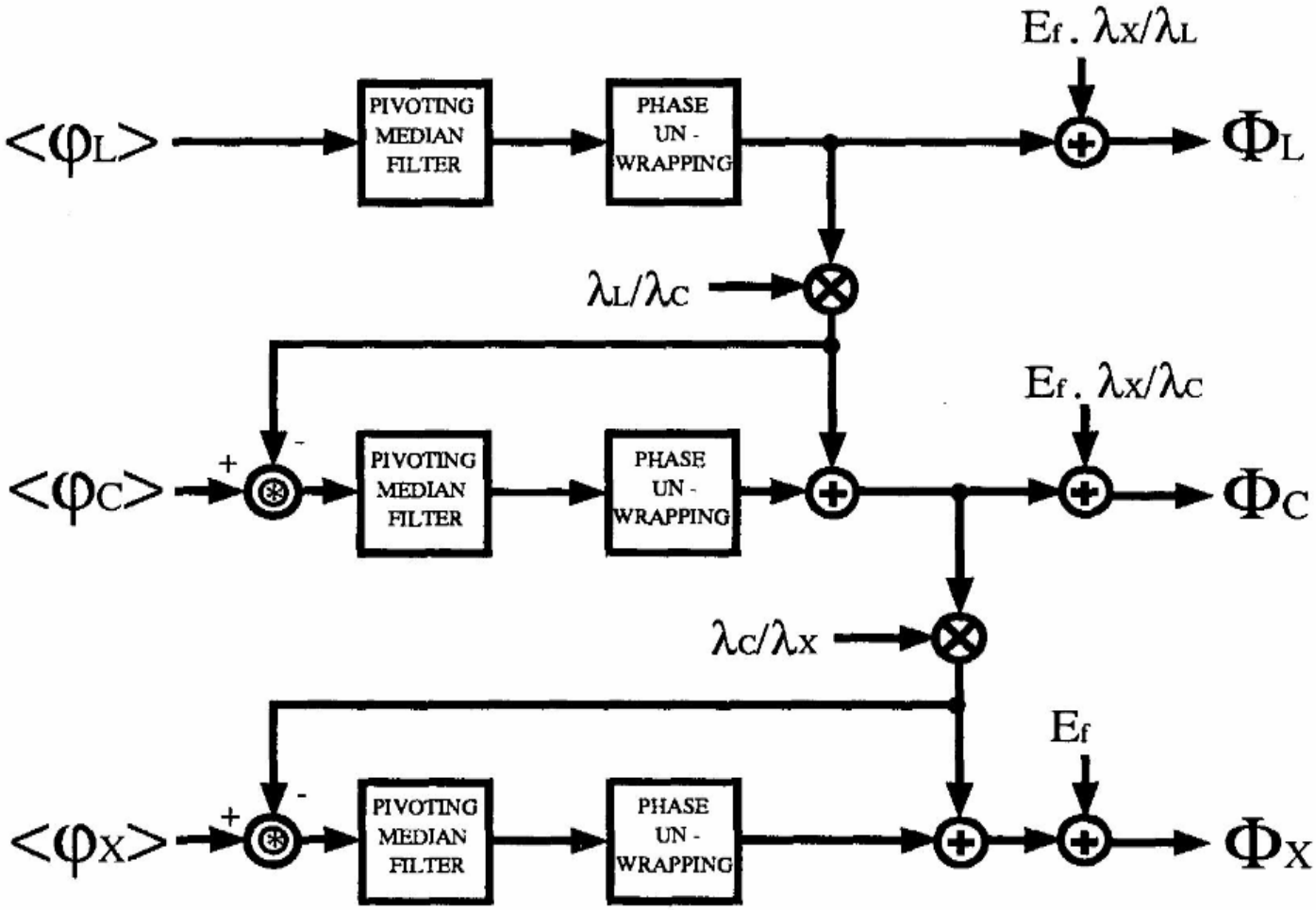

Scaling to X-Band for Comparision Purposes

Quellenangabe

Multifrequency Phase Fusion Scheme

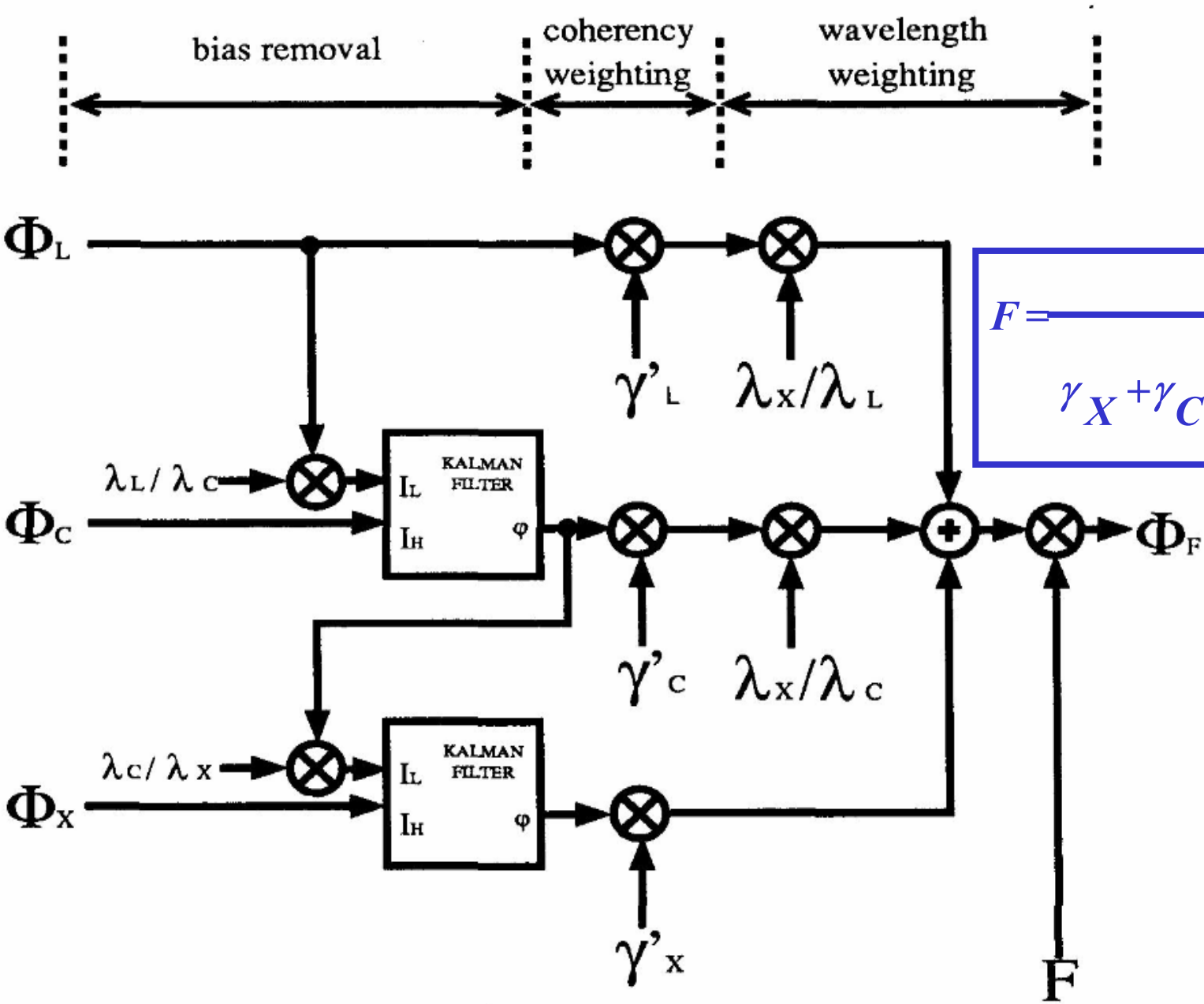

$$F = \frac{1}{\gamma_X + \gamma_C \left(\frac{\lambda_X}{\lambda_c}\right)^2 + \gamma_L \left(\frac{\lambda_X}{\lambda_L}\right)^2}$$

Effect of Filtering

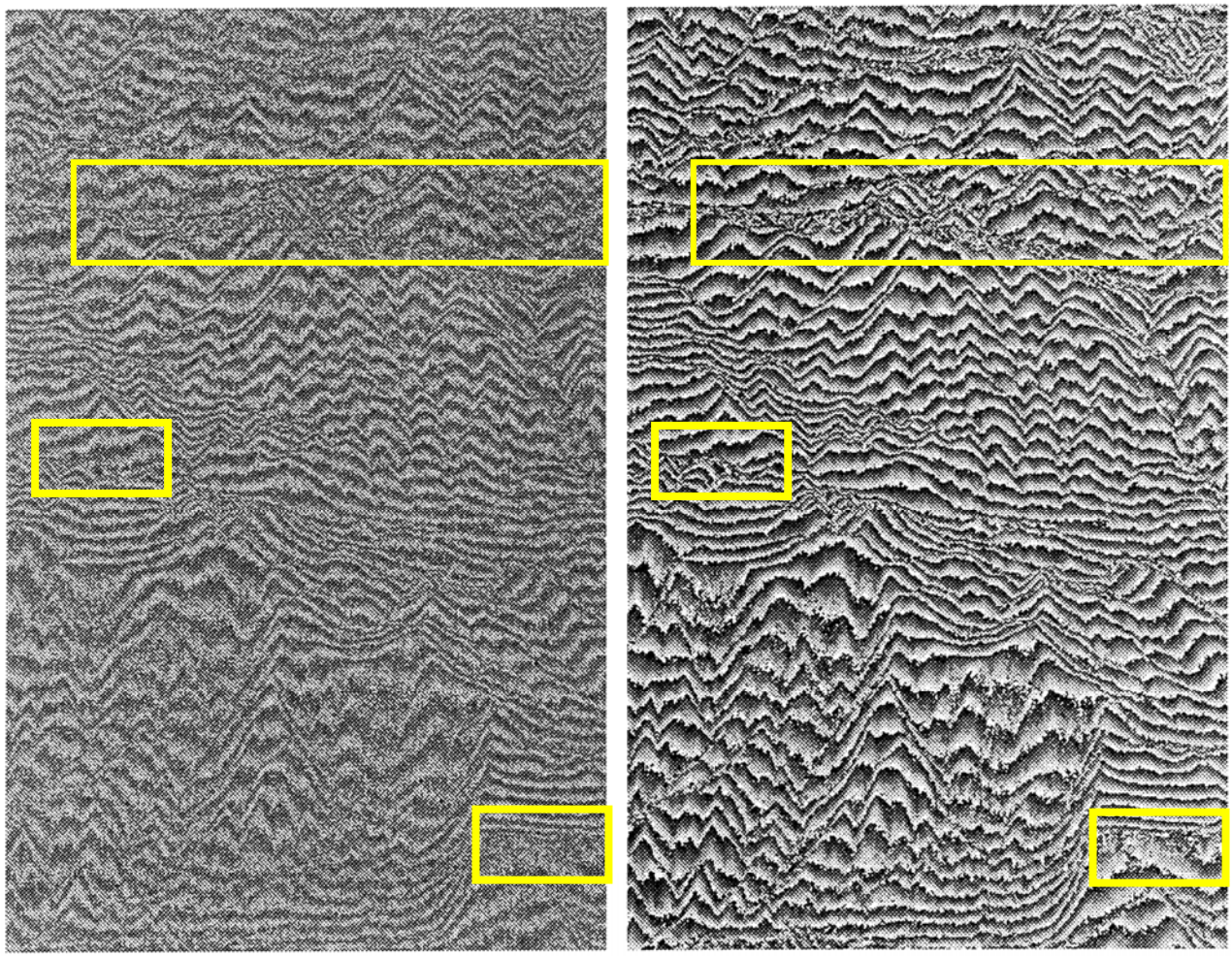

unfiltered filtered

Quellenangabe

Multifrequency evaluation: Unwrapped Phase Profiles

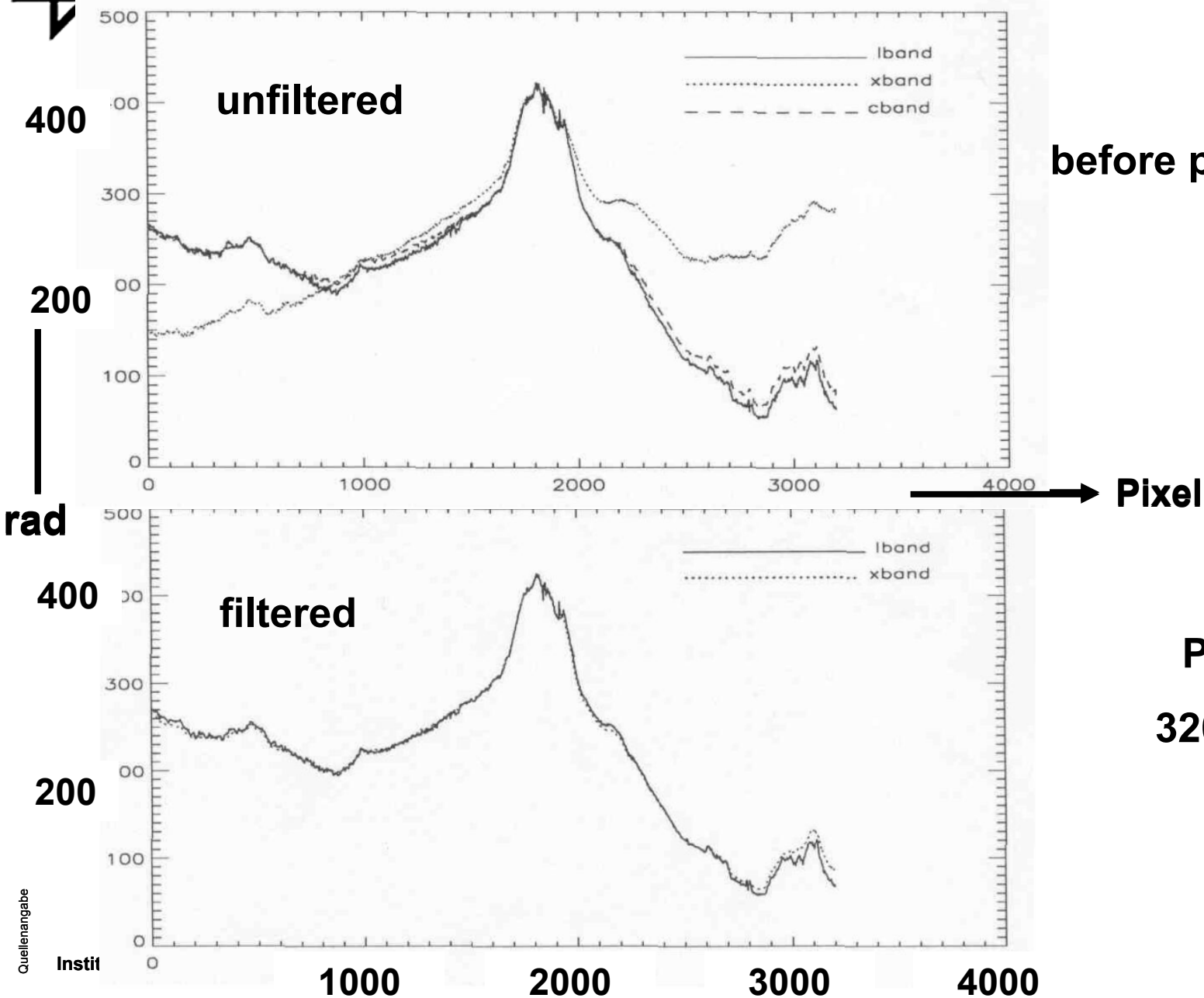

Filtering

before phase unwrapping

Pixel Size: 21 m

3200 Pixel ~ 67 km

2π ~

Quellenangabe

Instit

Main Features considered in the Fusion Algorithm

Features	X-Band	C-Band	L-Band
Bias	yes	yes	no
Coherence over areas without vegetation	high	high	high
Coherence over areas with sparse vegetation	low	medium	high
Coherence over areas with dense vegetation	low	low	high
Height standard deviation	2,5 m	4,5 m	19 m

Quellenangabe

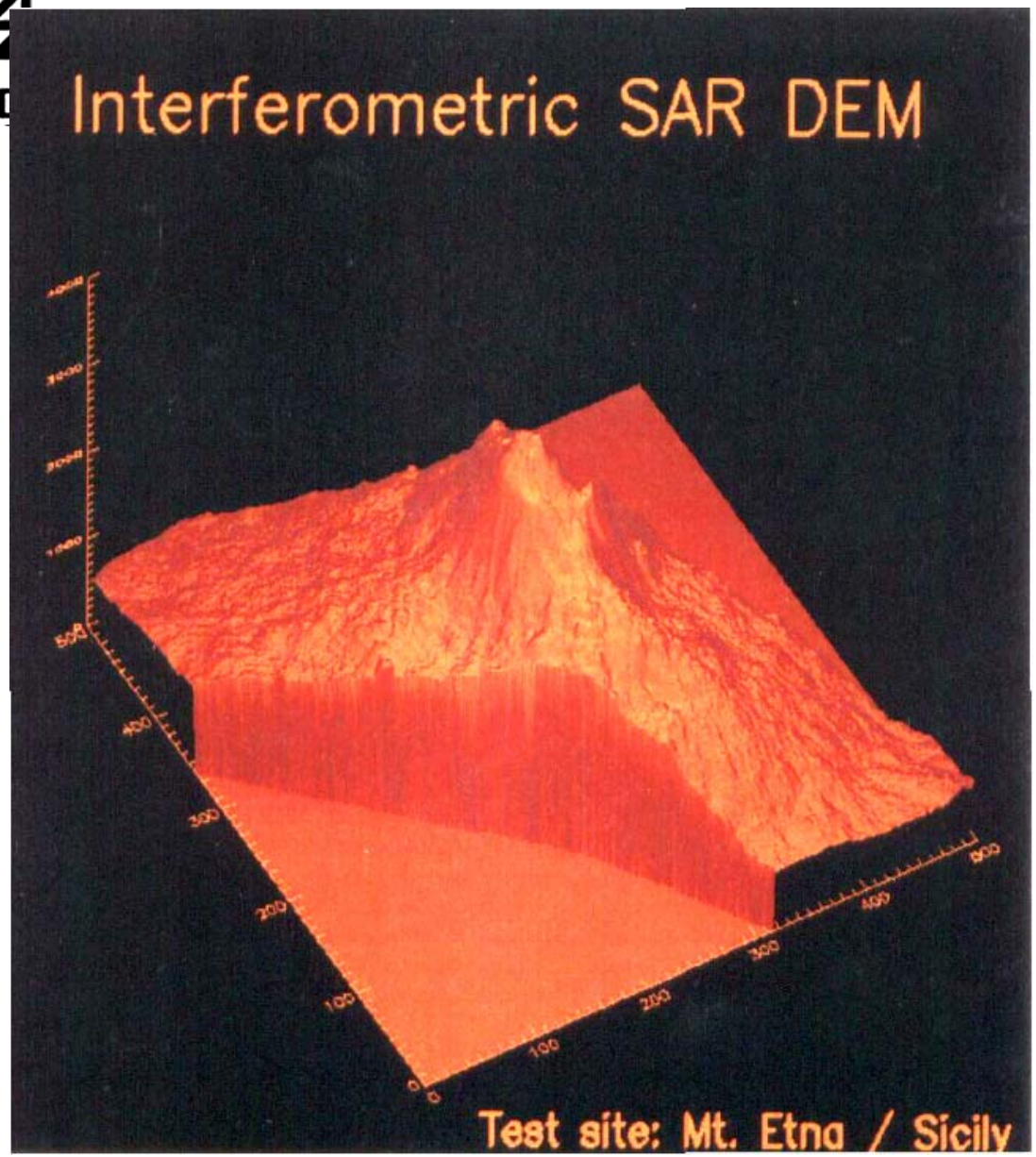

$$\Delta z_{\Phi} = \frac{\lambda R_0 \sin\vartheta}{4\pi B \cos(\vartheta - \xi)} \Delta\Phi$$

$\Delta\Phi = 12°$; $\gamma_L = \gamma_L = \gamma_L = 0{,}9$

SNR > 10 dB

$\vartheta = 49°$; B = 54 m; $\xi = 41°$

R = 316 km

$\Delta\Phi = 2\pi$

$\Delta z_{\lambda} = \lambda$ 2,23 km

$\Delta z_L = 512$ m

$\Delta z_c = 111{,}5$ m

$\Delta z_x = 66{,}9$ m

Quellenangabe

Coherence and Phase Error Examples from SIR-C

Good coherence between 2 passes

X-Band: < 1 day

C-Band: < 3 days

L-Band: < 30 days

SNR	Phase Error $\Delta\Phi$ (rms)
10 dB	±40°
15 dB	±21°
20 dB	±13°
25 dB	±9°
30 dB	±4°

Ambiguity Ratio	Phase Error $\Delta\Phi$ (rms)
0 dB	±50,7 °
-10 dB	±12,8 °
-20 dB	±4,02 °
-50 dB	±0,13 °

Quellenangabe

Coherence Classification, Mt. Etna, Sir-C Data

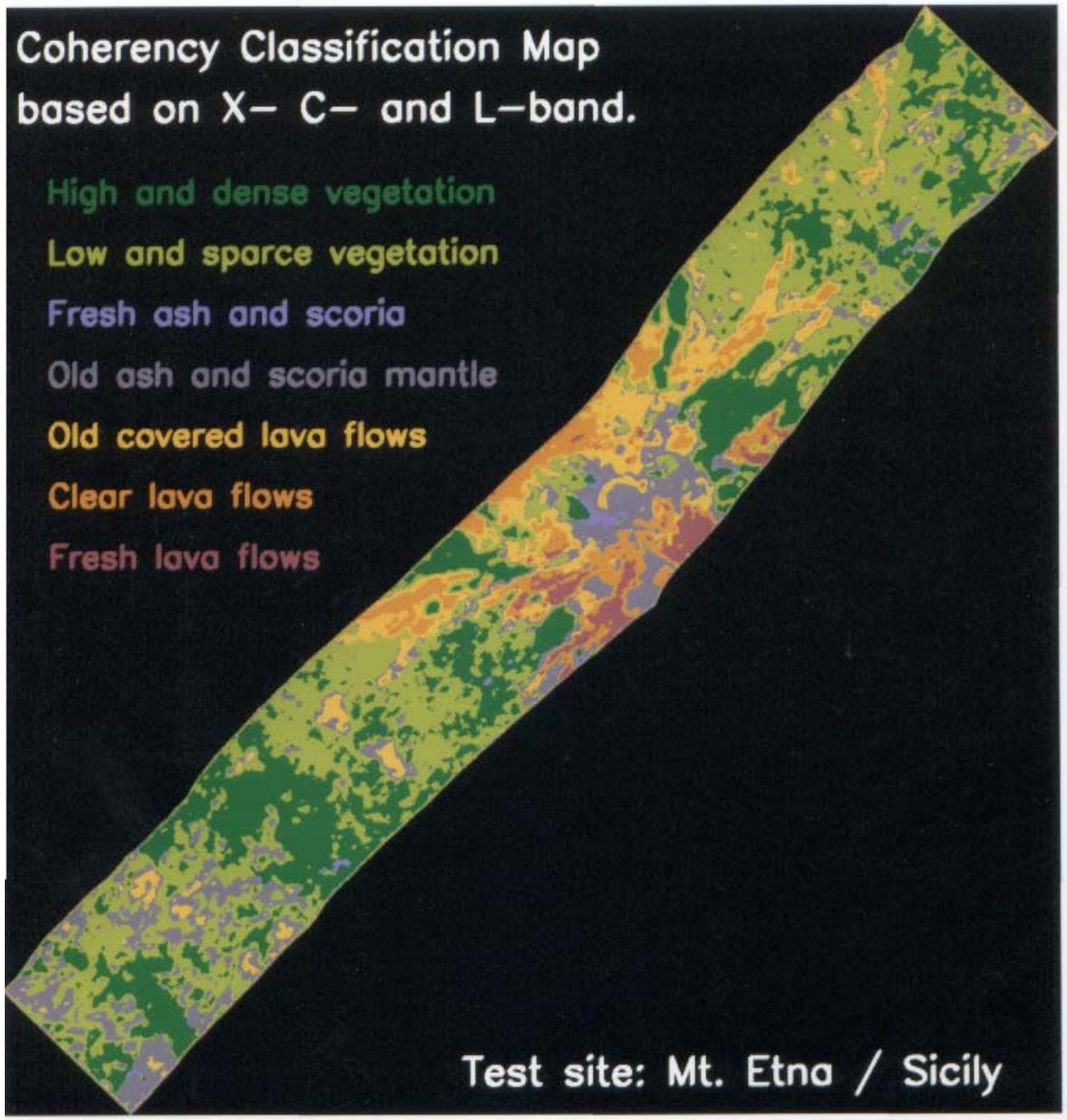

Quellenangabe